INVESTIGATION ON TOROIDAL PCB EMBEDDED INDUCTOR FOR POWER ELECTRONICS APPLICATIONS

by

Neel Mayur Shah

A thesis submitted to the faculty of
The University of North Carolina at Charlotte
in partial fulfillment of the requirements
for the degree of Master of Science in
Electrical Engineering

Charlotte

2015

Approved by:

Dr. Babak Parkhideh

Dr. Badrul Chowdhury

Dr. Jonathan Bird

© 2015
Neel Mayur Shah
ALL RIGHTS RESERVED

ABSTRACT

NEEL MAYUR SHAH. Investigation on PCB embedded inductor for power electronics applications.
(Under the direction of DR. BABAK PARKHIDEH)

This thesis investigates a Printed Circuit Board embedded air core inductor at 5 MHz switching frequency for two different prototypes $200W - 5A/250nH$ and $300W - 10A/150nH$. The toroid structure has been used, as they have weaker external magnetic field compared to solenoid and spiral structure, hence, toroid structure has less Electromagnetic Interference (EMI) issues. This research focuses on thermal management of the proposed inductor for high current up to 10 A. The temperature rise remains in the maximum range of $40°C$ without using a heat sink. Furthermore, finite element analysis was used to predict the temperature rise, resistance and inductance value. Then, hardware for these prototypes was implemented to verify simulated results. Hardware was also tested for filtering purpose of H bridge converter.

To make a high performance inductor, an optimized design with $300W-18A/50nH$ and with lower resistance was also proposed and same experiments were performed. In this design, 4 oz copper was used to reduce DC resistance and temperature rise. For 18 A current, the temperature rise also stays below $40°C$.

Therefore, proposed prototypes offer many benefits, such as higher efficiency, better filtering capability and lower manufacturing cost, can be brought in future high frequency converters by reducing the size of the passive elements.

DEDICATION

This thesis is dedicated to my parents, Mayur Shah and Nayana Shah, my sister, Avani Gandhi and my brother in law, Shalin Gandhi.

ACKNOWLEDGMENTS

First, I would like to thank my advisor, Dr. Babak Parkhideh for throughout support, guidance and encouragement. I am grateful for his trust and giving me an opportunity to work with him.

I would like to thank my committee members, Dr. Badrul Chowdhury and Dr. Jonathan Bird, for spending time to assess my work and participating in my thesis.

I would like to thank JMAG Corporation for the use of their finite element analysis software.

I would like to thank Mr. Mehrdad Biglarbegian for his aspiring guidance, invaluably constructive criticism and friendly advice during the thesis.

I would like to thank my grandma, Anila Shah for her continuous moral support and guidance.

Lastly, I would like to thank my officemates, Behdad, Mahmoodreza, Iman and Saurabh, and my friends, Jinay, Ankit, Parita, Rima and Krisha for their support and great memories.

TABLE OF CONTENTS

LIST OF FIGURES

LIST OF TABLES

CHAPTER 1: INTRODUCTION

1.1 High Frequency Magnetic Materials

The ongoing demand to miniaturize consumer electronics requires smaller power supplies. Passive components such as inductors and transformers, occupy large space in power supplies. At higher frequency, due to inverse proportion of the passive components to switching frequency; in the case of constant ratio of the voltage and current, there is an opportunity to reduce the size of passive components [1].

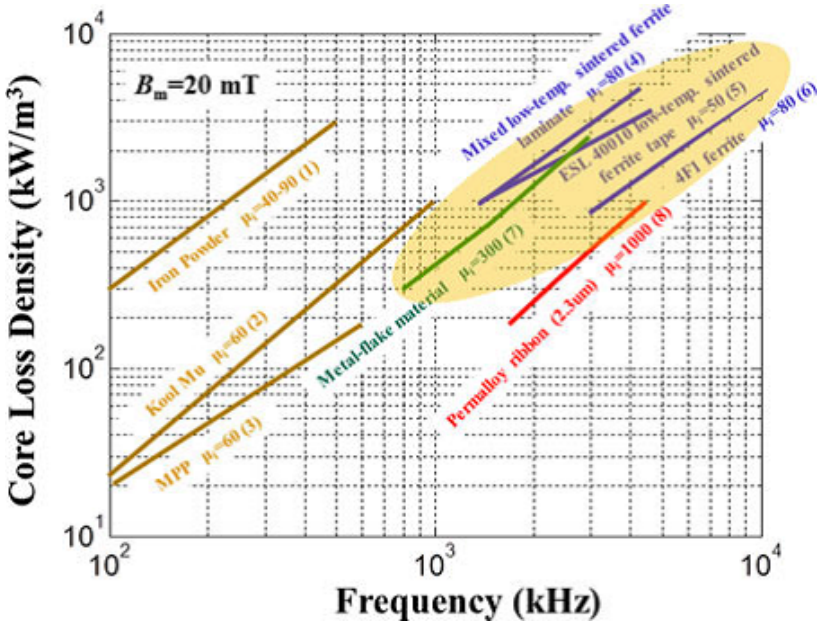

Figure 1.1: Magnetic core loss density for different magnetic materials

For high frequency (1 MHz to 10 MHz) inductors, conventional magnetic materials such as ferrite, Molly Permalloy (MPP), High Flux, Cool Mμ and iron powder, cannot be used due to higher core loss density and tending to be saturated at high currents. As shown in figure 1.1, core loss density of the iron powder and cool mμ material increases too high with frequency. The core loss density of permalloy ribbon

core is in the range to use at high frequency, but due to higher cost and sensitivity to mechanical stress, they cannot be used. Some ferrite composites, such as high-temperature sintered Ni-Zn ferrite, low-temperature sintered Ni-Cu-Zn ferrite, a mixed low-temperature sintered Ni-Cu-Zn multilayer ferrite and NEC-TOKINs metal-flake composite material, can be used at high frequency. Since NEC-TOKINs metal-flake composite material has lower core loss density compared to other Ferrite composites, it is one of the best option at high frequency [2]. However, at high frequency, lower values of passives are required, that means air core inductors can fulfill the requirement. As air core inductors do not have a core, core loss can be eliminated. Since, they do not have magnetic material, they are free from saturation problem. In addition to that, they are easier and cheaper to be manufactured compared to magnetic core inductors.

1.2 Motivation

In the air core inductors, air core solenoids are the most commonly used inductors. The comparison of Printed Circuit Board (PCB) embedded air core inductor and air core solenoid were well explained in paper [3]. Due to equivalent electric performance, concentrated magnetic flux inside the geometry, small volume and less material consumption, PCB embedded air core inductors have better characteristics than air core inductors.

The comparison of three different geometries of PCB embedded inductors were described in paper [4]. The spiral inductor has the highest quality factor and it is more flexible in comparison to toroidal and solenoid inductor. Due to the rectangular shape of the solenoid, it is easy to align on the PCB. However, spiral and solenoid inductor, both have strong external magnetic field outside their geometry, where as in the toroidal inductor, magnetic flux is restricted inside the geometry that means they have much weaker external magnetic field.

Due to much weaker magnetic external field, further investigation of the toroidal

inductor was done in this thesis. Two types of inductance generate from the toroidal geometry, one due to the field inside the toroid and another is due to a single loop around the center hole. The formula to calculate to inductance for a toroidal geometry is explained in paper [5]. The formula to calculate the resistance is formulated in paper [6].

In this thesis, three different kinds of prototypes of PCB embedded inductor were used to investigate mainly focused on the temperature rise for different switching frequencies and for various current values. The main advantage of these prototypes are that they do not require a heat sink to dissipate more heat, as they remain in the range for maximum temperature rise for the designed current and frequency. The value of the inductance and resistance of the geometries are obtained by an analytical calculation, simulation results and experimental results.

1.3 Organization of Thesis

Chapter 1 explains the introduction and motivation for this thesis.

Chapter 2 gives the background of different types of inductors, different types magnetic core and the losses in an inductor.

Chapter 3 explains the analytical calculation, provides simulation analysis and hardware results for the first two prototypes of the PCB embedded inductor.

Chapter 4 describes the design procedure and analysis of the optimized prototype of the PCB embedded inductor.

Chapter 5 provides discussion of all three prototypes. Finally, the summary and future work will be presented.

CHAPTER 2: BASICS OF INDUCTOR

2.1 Introduction

This chapter briefly explains the basics of inductors. Section 2.2 presents technical background of inductors. Different types of inductors are explained in section 2.3. Magnetic core inductors, air core inductors and PCB embedded inductors are presented in section 2.4, 2.5 and 2.6 respectively.

2.2 Technical Background of Inductor

Basically, a conventional inductor is a coil with two terminals which consists of a conductor such as a copper wire, which is wound around the coil. An inductor stores energy in a magnetic field when current pass through it. According to Faraday's electromagnetic induction law, the time varying magnetic field induces emf across a conductor, when the current passing through the wire changes.

The derivation of inductance is taken from Fundamental of Power Electronics by Robert W. Erickson [7]. When a magnetic flux $\boldsymbol{\phi}$ flows through a surface area A_c, the relation between magnetic flux $\boldsymbol{\phi}$ and magnetic flux density $\boldsymbol{B}$ can be expressed as

$$\boldsymbol{\phi} = \int \boldsymbol{B} \cdot \boldsymbol{dA} \tag{2.1}$$

where, $\boldsymbol{dA}$ is vector area element having direction normal to surface. When there is a uniform flux density,

$$\phi = BA_c \tag{2.2}$$

where dA is the enclosed cross section area of the loop. According to Faraday's

law of electromagnetic induction, when magnetic flux flows through a coil of wire as shown in figure 2.1, the induced emf can be described as,

$$v(t) = \frac{d\boldsymbol{\phi}(t)}{dt} \tag{2.3}$$

Substituting equation 2.2 into equation 2.3

$$v(t) = A_c \frac{d\boldsymbol{B}(t)}{dt} \tag{2.4}$$

where $\boldsymbol{\phi(t)}$ is flux flows through coil of wire, $v(t)$ is induce emf due to flux in coil and $\boldsymbol{B(t)}$ is flux density. When there is n number of turns in coil,

$$v(t) = nA_c \frac{d\boldsymbol{B}(t)}{dt} \tag{2.5}$$

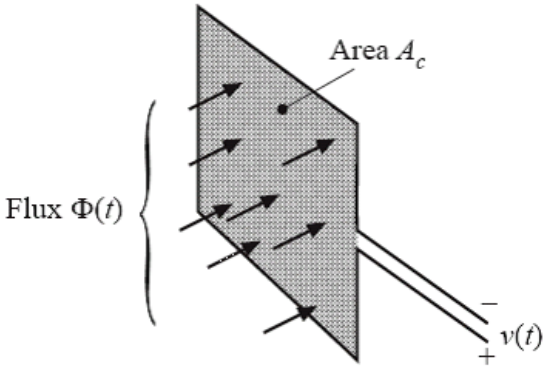

Figure 2.1: Faraday's law

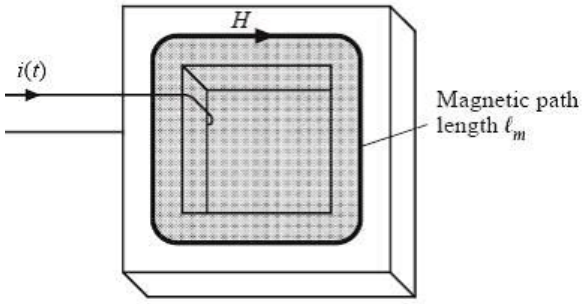

Figure 2.2: Ampere's law

According to Ampere's law as shown in figure 2.2, when current pass through winding, it induces magnetic field. The relation between magnetic field strength $\boldsymbol{H(t)}$ and current $\boldsymbol{I(t)}$ can be expressed as

$$\oint \boldsymbol{H(t)} \cdot \boldsymbol{dl} = \boldsymbol{I(t)} \tag{2.6}$$

where $\boldsymbol{dl}$ is vector length of flux path. When magnetic field strength is uniform in n

number of turns,

$$H(t)l_m = I(t) = ni(t) \tag{2.7}$$

where l_m is magnetic path length.

Now, magnetic flux density and magnetic field strength is related by,

$$B(t) = \mu H(t) \tag{2.8}$$

where μ is magnetic permeability, which can be measured in H/m. Magnetic permeability is defined as, $\mu = \mu_0\mu_r$, where μ_r is relative permeability of material and μ_0 is permeability of air which is equal to $4\pi \times 10^{-}7H/m$. Replacing $B(t)$ into equation 2.5 from equation 2.8

$$v(t) = \mu n A_c \frac{d\boldsymbol{H}(t)}{dt} \tag{2.9}$$

Substituting $H(t)$ from equation 2.6 to 2.9

$$v(t) = \frac{\mu n^2 A_c \, di(t)}{dt} \tag{2.10}$$

From circuit theory the voltage, created by current across the inductor can be expressed as

$$v(t) = L\frac{di(t)}{dt} \tag{2.11}$$

Comparing equation 2.10 and equation 2.11

$$L = \frac{\mu n^2 A_c}{l_m} \tag{2.12}$$

where L is inductance, characteristics of inductor, can be measured in Henry (H).

2.3 Different Types of Inductors

Inductors are used in many different applications, for instance to filter out specific frequency, in Switch Mode Power Supplies, energy storage, radio reception and transmission, etc. For each application, different types of inductors are required. In some applications, low or high inductance, small core size, high or low power inductors are required.

For that, in industries, the following inductors are available.

(a) Magnetic Core Inductor

(b) Air Core inductor

(c) PCB Embedded Inductor

2.4 Magnetic Core Inductors

These types of inductor cores are mainly made from soft magnetic material, which is a sub category of ferromagnetic material. In this type of core, high value of inductance (in range of μH to H) can be achieved by selecting high permeability core material. But, with the high permeability core losses will increase as well. So, there is always a compromise between inductance and losses. There are different materials, such as Ferrite, Iron Powder, MPP, High Flux, Kool μ, Xflux, available in the market. The type of material also depends on the particular application in which some require low core losses, higher saturation point, and high switching frequency. This type of inductor cores are available in different shapes for instance Toroid, E, POT, ER, EP, I, U and RM as shown in figure 2.3 [8]. The main advantage of magnetic core is that it can restrict magnetic flux inside the geometry, therefore magnetic path length can be predictable. Magnetic path length is also an important factor to calculate inductance.

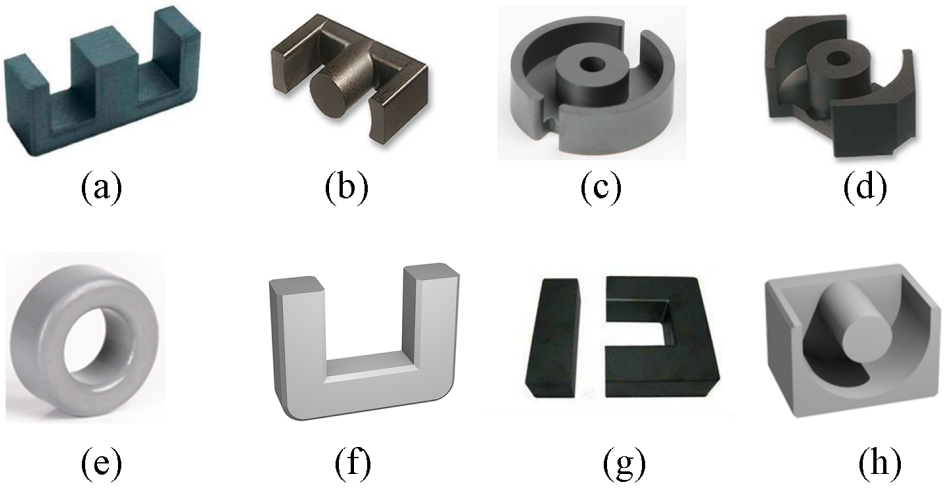

Figure 2.3: Different types of magnetic cores: (a) E core, (b) ER core, (c) POT core ,(d) RM core, (e) Toroid Core, (f) U core, (g) UI core and (h) EP core

2.5 Air Core Inductors

Air core inductors are usually made without core or with non-magnetic core like plastic, ceramic etc. These type of inductors are free from core losses, as they do not have core. They have lower inductance values compared to magnetic core, because the relative permeability of air is only one, which is very small compared to magnetic material. Because of their lower relative permeability, at the same inductance value, air core inductors occupy more space compared to the magnetic core inductor. Due to lower inductance and lower losses, these type of inductors are suitable for high frequency applications, as lower values of inductance is needed at high frequency. However, at high frequency, for the loss calculations, skin effect, proximity effect and parasitic need careful consideration. Due to this effect, at high frequency the resistance of the conductor will increase, which results in higher losses. To reduce skin effect and proximity effect litz wire can be used.

2.6 PCB Embedded Inductors

Inductors can be embedded within a PCB with magnetic core and without magnetics which is air core. For instance, ferrite polymer compounds or electroplated CoNiFe, NiFe can be used as magnetic material and PCB embedded magnetic core inductor [10]. Due to the benefits explained in section 2.5, PCB embedded air core inductors have better performance. There are many different geometries that exist for PCB embedded inductors, however spiral, solenoid and toroid inductors are most commonly used. These types of inductors have their pros and cons which will be explained briefly in section 3.3.

Other than these types of inductors, the research about inductors on low temperature co-fired ceramic, on magnetic substrates and on magnetic coated bond wires, etc are on going [10].

2.7 Losses in Inductors

There are mainly two types of losses, copper losses and core losses. Copper loss occurs due to the resistance of the wire or conductor and generates heat when DC or AC current flows in the wire. It can be calculated as shown in equation 2.13.

$$Copperloss = I^2R \tag{2.13}$$

where I is DC or RMS current and R is the resistance of wire.

At high frequency, the alternating current (AC) has a tendency to pass on the outer surface of the conductor. This effect is called the skin effect. Due to the skin effect the resistance will increase, as they have lower space to cross the conductor [11]. The skin depth decreases when frequency increases, that means resistance increase. The skin depth is defined as shown in equation 2.14.

$$\delta = \sqrt{\frac{2\rho}{2\pi f \mu_r \mu_0}} \tag{2.14}$$

where ρ is resistivity of conductor, f is frequency, where μ_r is relative permeability of material and μ_0 is permeability of air.

The core loss is one of the main factors to be considered when designing a magnetic core inductor, which can be calculated by Steinmetz equation as shown in equation 2.15. It depends on the magnetic material, material thickness, magnetic flux density, frequency and operating temperature. Due to direct proportion to frequency, core loss increases with the frequency [11]. Among all the powder core, the MPP core has the lowest core loss [12].

$$P_{fe} = K_c F^{\alpha} B_{max}^{\beta} \tag{2.15}$$

where B_{max} is magnetic flux density, F is frequency; K_c, α and β are constants which can be found on core data sheet and in the range of 0.053 to 16.9, 1.25 to 1.81 and 1.74 to 2.35 respectively. The magnetic flux density is in the range of 0.3 to 1.5, which will decrease at higher frequencies. Basically, magnetic flux density needs to be chosen in such a way that magnetic core should not saturate, since in saturation relative permeability of magnetic material reaches to permeability of air and magnetic core can store less energy (i.e. inductance value will decrease). The saturation flux density also depends on the temperature, it decreases as temperature increases. Each material has a curie temperature which can be defined as, at certain temperature ferromagnetic materials change their property and become paramagnetic material [11]. The curie temperature for different material is in the range of $135°C$ to $700°C$ [8][9].

2.8 Quality Factor of Inductors

Quality factor is another important parameter of an inductor which can be calculated as shown in equation 2.16. Usually, it helps to determine the effectiveness of an inductor, as the quality factor mainly depends on the inductance, resistance and frequency. The resistance increases at higher frequency due to the skin effect and

proximity effect. For an inductor, a higher Q is better, as resistance will be lower [7].

$$Q = 2\pi \times \frac{stored\,energy}{energy\,dissipated\,per\,cycle} = \frac{2\pi f L}{R} \tag{2.16}$$

CHAPTER 3: DESIGN AND SIMULATION

3.1 Introduction

This chapter explains the analytical design of the proposed PCB embedded air core toroid inductor for the calculation of inductance, resistance and temperature rise. A Finite Element Analysis (FEA) is then conducted for the proposed design to investigate different characteristics, for that JMAG software package has been utilized. JMAG is known for FEA to analyze multi-physics simulations like electromagnetic, thermal, and electric [13]. For FEA modeling, JMAG designer version 13.1 has been used in this thesis. In the following section 3.2, a comparison of different structures of PCB embedded air core inductors is described.

3.2 PCB Embedded Air Core Inductors

For operation at the same level of the voltage and the current ratio, the capacitor and the inductor values inversely proportional to the switching frequency. In other words, switching at the higher frequency along with some challenges brings a good opportunity to reduce the inductor size, which can result in lower losses. However, core losses and winding losses (in alternating current system) are a major contribution to the losses of magnetic-core inductors which are directly proportional to the frequency, thus rendering them inefficient for high frequency applications [14]. Yet, air-core inductors overcome this disadvantage, as they can be designed without core or with non-magnetic core, for instance with plastic, ceramic or glass; they are free from core losses. Other than that, they are cheap, easy to manufacture, same characteristics with different temperatures and independent of current that means they do not saturate at high current[15]. At the same time, these types of passive elements (inductors) have

some challenges to overcome such as electromagnetic interference (EMI), parasitic capacitance and to design high Q inductors at high frequency [3][4][16]. The relative permeability of an air core inductor is only one which is very small compared to the magnetic core inductor, more number of turns or large volume are required to get high inductance value. Hence, air core inductors can be used at high frequency where lower inductance is required. For air-core inductor, a solenoid is mostly used, however, PCB embedded air-core inductors have advantages over them as stated below [3].

(a) Better electrical performance

(b) Higher containment of magnetic flux inside the geometry

(c) Lower volume

(d) Directly embedded to PCB

(e) Less material consumption

Some of the PCB embedded air core inductors are most commonly used in many articles [3][4][17], which can be described as below:

(i) Spiral Inductor:

As shown in figure 3.1, the design of spiral inductor can be very flexible since it can be designed in single layer or multiple layers and in circular, hexagonal, octagonal and square shape [17]. It has the highest quality factor among these three structures and these types of inductors are mainly used in integrated circuits [4].

(ii) Solenoid Inductor:

As shown in figure 3.2, a solenoid inductor can be designed in rectangular shape, which is very appropriate in PCB. As many components on PCB are in rectangular shape, this type of inductor does not need any special space

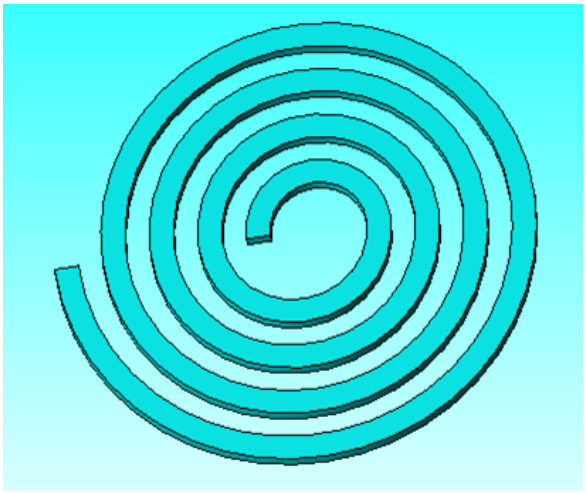

Figure 3.1: Spiral inductor

on the board. Another benefit of solenoid is that both of the terminals can be designed in the same layer [4].

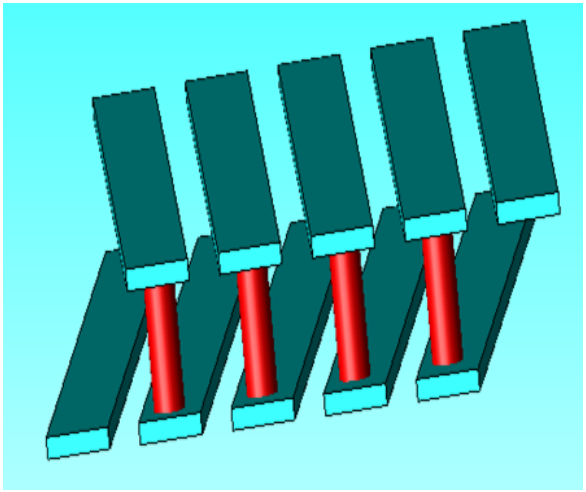

Figure 3.2: Solenoid inductor

(iii) Toroid Inductor

As shown in figure 3.3, toroid inductor has more number of vias than previous two structures do; therefore, this geometry is not as flexible as the spiral and solenoid type. However, the outer diameter and inner diameter can be adjusted according to the requirements of inductance and resistance. Due to toroid geometry, the magnetic flux can be restricted inside the geometry which

helps to eliminate EMI issues, which is a problem for the other two structures [4].

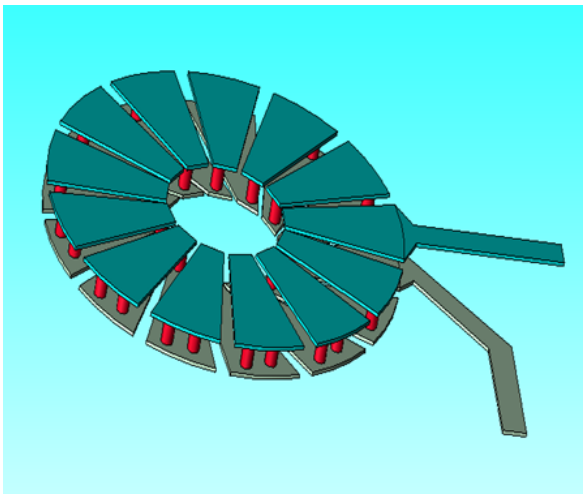

Figure 3.3: Toroid inductor

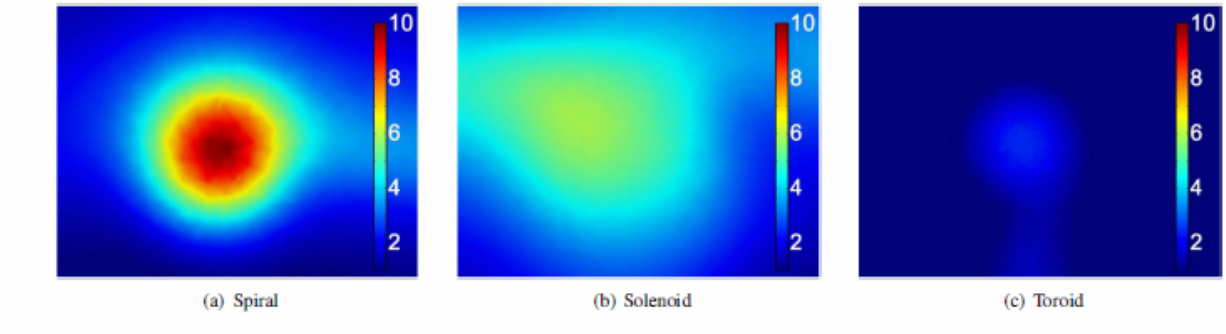

Figure 3.4: Magnetic field (A/m) $2mm$ above of PCB embedded air core inductors [4]

Now, if we compare these three structures, the toroid inductor has the lowest resistance and least flexible geometry among all of them. Figure 3.4 presents simulation of magnetic field above 2 mm of structure is described, in which red color is hot spot. That means, the spiral, solenoid, toroid inductor have highest, medium and lowest magnetic field respectively. That means toroid has much weaker external magnetic field compare to the other two geometries. This external magnetic field causes EMI problem which affects the component near the inductor and the whole performance

of the circuit board [4]. Due to this fact, in this thesis, further investigation of the toroid inductor was done for thermal management for high power and the calculation of inductance and resistance.

3.3 PCB Embedded Air Core Toroid Inductor

The proposed geometry of this type of inductor is as shown in figure 3.5 which can be designed with two copper layers at some distance and each layer needs to be designed as petals which can be connected with a number of vias. The di-electric material between two copper layers is FR-4 (flame retardant) which is used in most of the PCB. The current enters from input and flows through the connected top petal up to inner side. Then, current reaches to the bottom petal through the inner side via. The current crosses bottom petal till outer side via, through outer side via current goes to top side second petal as outer side vias are connected to another petal of top side. This strategy will be applied in whole toroid, so that way current can flow in whole toroid in number of series loops. The series loops can be considered as number of turns. Inductance can be determined with the help of the area of the loops and number of loops [3].

3.4 Analytical Design

In this section, the explanation for selecting parameters, and formula for inductance and resistance are discussed.

The state of art in today's market, thanks to very low input gate charge of NexFET MOSFET and GaN switches, which are the best candidate for low voltage application and low loss at 500 kHz with the combination of optimized control methods such as unipolar PWM switching, the switching loss can be reduced by up to 3%. However, the passive components such as inductors due to the saturation limit of the magnetic at high switching frequency operation are not fully developed. Hence, our first goal is to design a PCB embedded inductor suitable for high frequency (5 MHz) and for

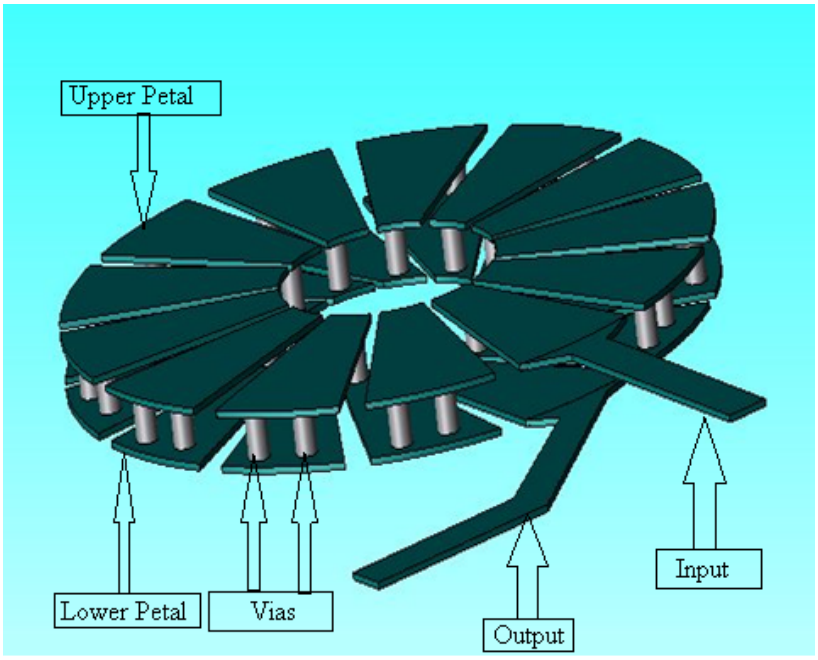

Figure 3.5: Basic geometry of PCB embedded inductors

high current ($10\,A$), as the typical range of power for each solar panel is around $200\,W$ to $325\,W$ [18]. The approximate value of inductance can be calculated from the cutoff frequency equation as shown in equation 3.1, where cutoff frequency is $1/10^{th}$ of the operating frequency [7]. According to the current ripple calculation, less than $10\,\mu F$ capacitance is required. Therefore for simplicity and to minimize the losses, $1\,\mu F$ of capacitance was selected. This means the value of inductance should be between $100 - 200\,nH$. Due to the many different parameters, initially the outer diameter and number of turns needs to be assumed.

$$f_0 = \frac{1}{2\pi\sqrt{LC}} \tag{3.1}$$

where L is inductance and C is capacitance.

$$Ampacity = kT^bA^c \tag{3.2}$$

where $k = 0.048$, $b = 0.44$, $c = 0.725$, T is temperature rise ($^\circ C$) and A is area ($mills^2$)

which is equal to $\pi\times$(Inner diameter + Plating thickness)$\times$Plating thickness, here thickness and diameter are in *mills*.

The vias, due to its highest resistivity and smallest area compared to petals, are vulnerable to pass the high current. Therefore, after considering the ampacity of filled vias, to pass 10 A current and maximum temperature rise of 40°C, diameter of vias can be calculated as shown in equation 3.2 [19]. From the diameter of the vias, the length of the inner side of the petal can be designed. Moreover, based on the inner side length of petal, distance between each petal and number of turns, the circumference of inner circle can be calculated. Due to the geometry restrictions, distance between each petal has to be maintained according to each geometry. Hence, diameter of inner circle can be found. Then, several numeric iterations have to be accounted in equation 3.3 to deduce the exact value of outer diameter, height and number of vias needed to achieve the required inductance and resistance. Number of turns and height are the main parameters to increase the inductance value, however resistance of inductor will increase in parallel with inductance. Therefore, there is always a trade-off to get low resistance and high inductance. Higher inductance can be achieved by increasing height, but there are some limitations such as the increase of cost and volume of inductor.

For the inductance calculation, first condition is assumed that the cross section of geometry should be rectangular. In this inductor, two types of inductance will generate. One inductance is due to magnetic field inside of geometry and another inductance is due to single turn loop around center hole of geometry[16].

The inductance of toroidal inductor can be determined by following formula [5],

$$L = \frac{N^2 h \mu_0}{2\pi} \ln(\frac{d_0}{d_i}) + \frac{d_i + d_o}{4}\mu_0[\ln(8\frac{d_0 + d_i}{d_0 - d_i}) - 2] \tag{3.3}$$

In power stage design, in order to reach high performance of the converters, having high efficient inductors/capacitors are key. Therefore, design of these elements with

the lowest resistivity, which results in lower losses, is critical. For calculation of DC and AC resistance, some conditions have to be assumed for approximate answers. The current is trying to pass on the inner edges and for calculation of whole resistance, resistance of petals and of vias have to be calculated separately. Both resistance can be calculated by following formula [4],

DC resistance for each petal;

$$R_{DC,petal} = \frac{\rho N}{2\pi T_{trace}} \ln(\frac{\pi d_0 - C_{trace}N}{\pi d_i - C_{trace}N}) \tag{3.4}$$

AC resistance for each petal;

$$R_{AC,petal} = \frac{\rho N}{2\pi \delta} \ln(\frac{\pi d_0 - C_{trace}N}{\pi d_i - C_{trace}N}) \tag{3.5}$$

where ρ is resistivity of material which is $1.68 \times 10^{-}5\,\Omega/mm$, N is number of turns, T_{trace} is thickness of copper, C_{trace} is distance between each petal, d_i and d_o is inner diameter and outer diameter respectively and δ is skin depth which is around $30\,\mu m$ at $5\,MHz$ can be calculated as shown equation 2.14. The DC and AC resistance of the vias can be calculated as shown below.

DC resistance for each via;

$$R_{DC,via} = \frac{\rho h}{2\pi T_{via}(D_{via} - T_{via})} \tag{3.6}$$

AC resistance for each via;

$$R_{AC,via} = \frac{2\rho h}{\pi \delta(D_{via} - \delta)} \tag{3.7}$$

Total DC resistance of inductor;

$$R_{DC} = N(2R_{DC,slab} + \frac{R_{DC,via}}{N_{inner}} + \frac{R_{DC,via}}{N_{outer}}) \tag{3.8}$$

Total AC resistance of inductor;

$$R_{AC} = N(2R_{AC,slab} + \frac{R_{AC,via}}{N_{inner}} + \frac{R_{AC,via}}{N_{outer}}) \tag{3.9}$$

After, the first design, second inductor was designed with the same outer and inner diameter, but for low power application with 5 A current to investigate the performance for lower profile inductor. The parameters of these prototypes can be tabulated as shown in table 3.1.

Table 3.1: Parameter of inductors

Parameters	**Design 1**	**Design 2**	**Units**
L	150	242	nH
N	13	26	$-$
d_o	60	60	mm
d_i	20	20	mm
R_{DC}	30	140	$m\Omega$
R_{AC}	47	228	$m\Omega$
d_{via}	2	1	mm
h	3.6	1.6	mm
ρ	$1.7 \times 10^{-}5$	$1.7 \times 10^{-}5$	$\frac{\rho}{mm}$
T_{trace}	0.035	0.035	mm
C_{trace}	2	1.5	mm
$number\ of\ vias$	37	76	$-$

As shown in table 3.1, when the number of turns increases, the inductance will increase. However, the resistance of inductor will increase, which makes an inefficient inductor. To design this type of inductor, the ratio between outer diameter and inner diameter, height, diameter of vias and number of turns play very important role. T_{trace} is the thickness of layer which relates directly with resistance, which means if T_{trace} is higher, DC resistance will be lower. However, AC resistance depends on skin depth at high frequency and the board will be more expensive for higher thickness of layer. The C_{trace} is restricted by geometry, as one petal should not conflict to other petal. Therefore, it can be concluded that the selection of number of turns and height of

the inductor is very crucial to achieve the appropriate value of the inductance and resistance. Higher T_{trace} helps to reduce the DC resistance and C_{trace} is restricted by geometry. The multi-physics simulations for thermal analysis and for calculation of inductance and resistance are explained in next section.

3.5 Basics of JMAG

JMAG is a simulation software, which is well known for FEA analysis for electro-magnetic and electro-mechanical simulations [13]. The basic steps of JMAG can be explained as shown in figure 3.6.

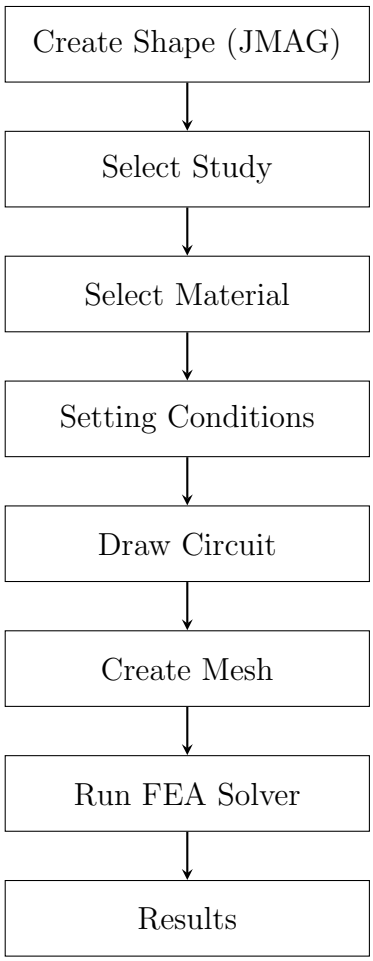

Figure 3.6: Basic steps of JMAG

As shown in figure 3.6, the geometry needs to be created or chosen from the library as per requirement. The different studies like magnetic, electric, thermal,

thermal stress and structural can be investigated for transient, static and frequency analysis. For various purposes, different materials are needed which can be found in JMAG library and the user can make customized material as well. For each analysis, particular condition needs to be set. For instance, to investigate current density symmetry condition and FEM conductor conditions, has to be set in JMAG. In some application, circuit is required for geometry to provide parameters like current, voltage, heat source etc. After that, mesh has to be assigned for geometry. Different mesh sizes can be assigned for different parts of geometry. After following all of steps FEA solver needs to be run for results. Different contour plots, flux line, vector plots and parameters can be found from the results to investigate further details.

3.6 Simulation Analysis and Results

Initially, in this thesis, two geometries with 13 turns and 26 turns of PCB embedded inductors as shown in figure 3.7 and 3.8 respectively, are investigated for the calculation of inductance and resistance, and for temperature rise at high current. For each analysis, different studies need to be selected and copper is used as a material in every case.

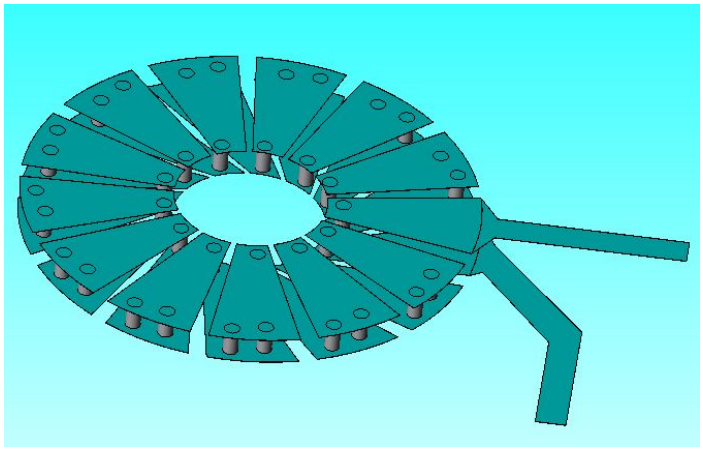

Figure 3.7: $N = 13, L = 150nH$

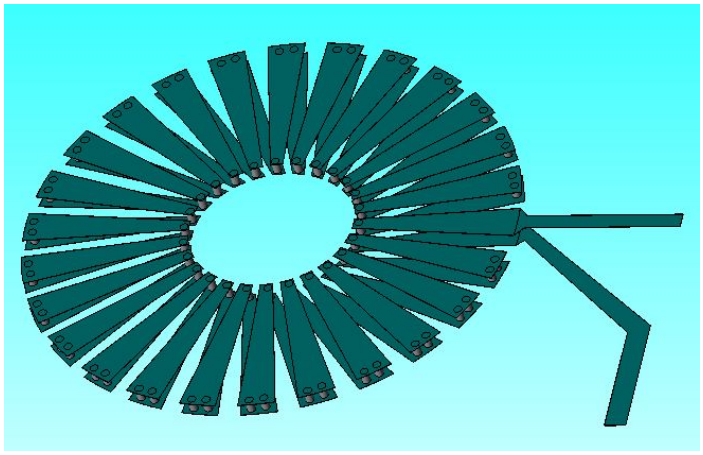

Figure 3.8: $N = 26, L = 240nH$

3.6.1 Calculation of Inductance and Resistance

The magnetic frequency analysis was done, as our interest is to find out the inductance and resistance value in frequency range of 1 MHz to 10 MHz. All the needed settings for this analysis is explained below:

(i) Designed geometry of 13 and 26 turns inductor in geometry editor.

(ii) Copper is used as a material for every parts.

(iii) Symmetry condition and conductor condition have to be defined on the outer end face of input and output as shown in figure 3.9.

(iv) Basic circuit of current source and inductor has been drawn. (as shown in figure 3.10)

(v) Mesh will be created by using default settings of JMAG.

(vi) The frequency range is defined from 1 MHz to 10 MHz.

(vii) Run the magnetic frequency study.

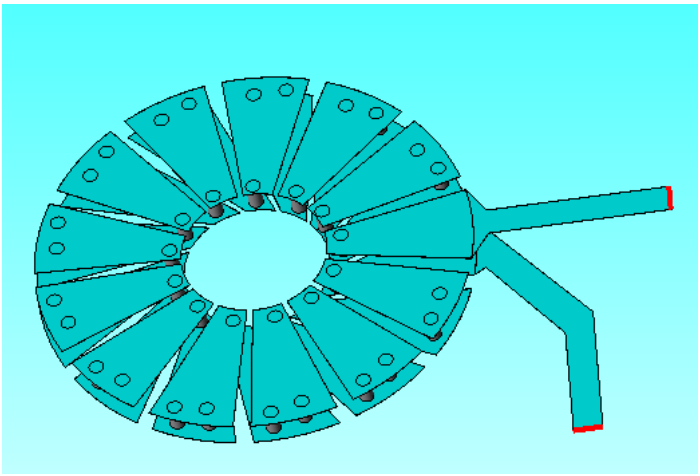

Figure 3.9: Inflow and outflow of inductor

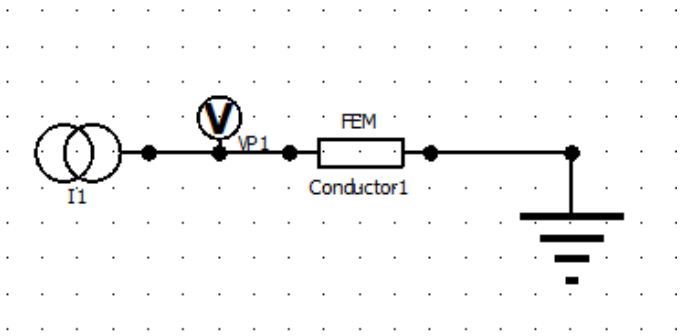

Figure 3.10: Basic circuit

After these steps, the imaginary part and real part of current and voltage can be extracted from the result section. From these values of current and voltage, the inductance and resistance can be calculated as shown below [20]:

$$R + j\omega L = \frac{Re(V) \cdot Re(I) + Im(V) \cdot Im(I)}{Re(I)^2 + Im(I)^2} + j\frac{Im(V) \cdot Re(I) + Re(V) \cdot Im(I)}{Re(I)^2 + Im(I)^2} \tag{3.10}$$

where $Im(V)$ and $Re(V)$ are imaginary and real part of voltage applied to inductor, $Im(I)$ and $Re(I)$ are imaginary and real part of current flowing through inductor, respectively. ω is angular frequency which can be calculated as $2\pi f$, where f is operating frequency.

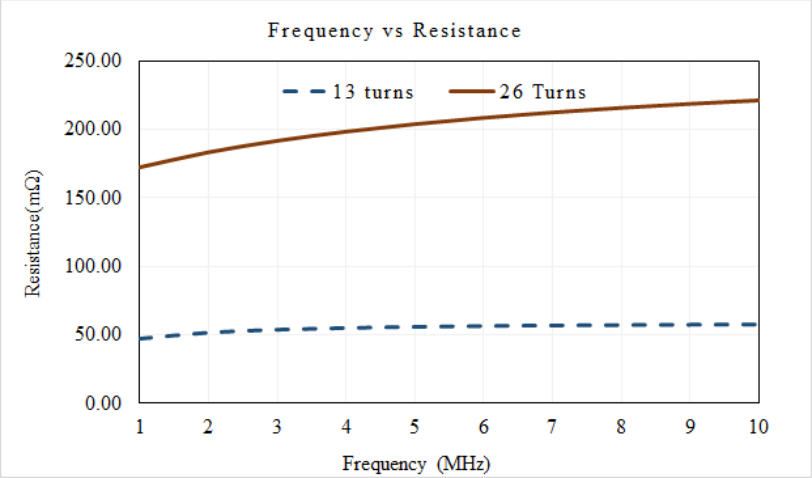

Figure 3.11: Frequency vs Resistance

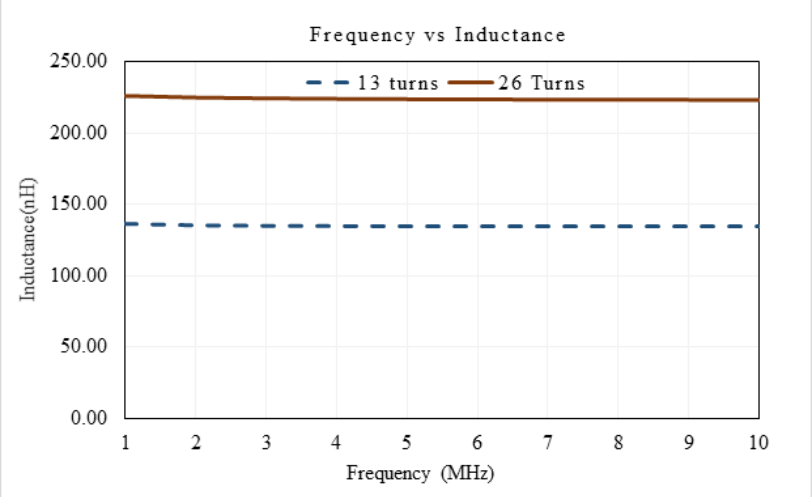

Figure 3.12: Frequency vs Inductance

As expected, the resistance and inductance is lower in the case of the design-1 with 13 turns than $design-2$ with 26 turns, since the number of turns are higher in 26 turns. As shown in figure 3.11, resistance starts increasing at higher frequency due to the skin effect and proximity effect which comes into play at higher frequencies; however, inductance remains constant at higher frequencies as shown in figure 3.12. According to this analysis, the selection of number turns is crucial for inductance and resistance which depends on the application. The simulated value of inductance and resistance are near to calculated value as shown in table 3.1.

3.6.2 Thermal Analysis

Temperature rise of inductor while applying different current can be predicted by this analysis. Two types of studies needs to be performed, magnetic transient and thermal transient study, to figure out temperature rise of inductor. For the magnetic transient study, same steps till number V as explained in 3.6.1 have been followed and then, ran magnetic transient study. The generated amount of heat in this analysis for respective current is used into thermal analysis as heat source. After this study, thermal transient study needs to be investigated. The necessary steps for this study is explained below.

(i) Initial temperature have to be defined for whole geometry at room or ambient temperature.

(ii) Assign heat source to every parts. In this condition, iron loss distribution from magnetic transient study have been referred as heat source for thermal transient study.

(iii) Then, heat transfer boundary condition has been assigned for outer side faces of upper and lower petal and to vias. Thermal heat transfer coefficient needs to be specified in this condition to transfer the heat by each side of inductor, which can be calculated approximately as shown below.

$$Heat\,transfer\,coefficient = \frac{Thermal\,conductivity\,of\,material}{Thickness\,or\,length\,of\,board} \tag{3.11}$$

where unit of thermal conductivity is $w/m\ ^{\circ}C$, thickness in m and therefore, unit of heat transfer coefficient is $w/m^2\ ^{\circ}C$. The thermal conductivity of FR-4 material is around 0.25 $w/m\ ^{\circ}C$ [21].

For 13 and 26 turns, heat transfer coefficient is 8 and 16 $w/m\ ^{\circ}C$ respectively according to equation 3.11. The simulated temperature profile is shown below for both the inductors when passing different currents.

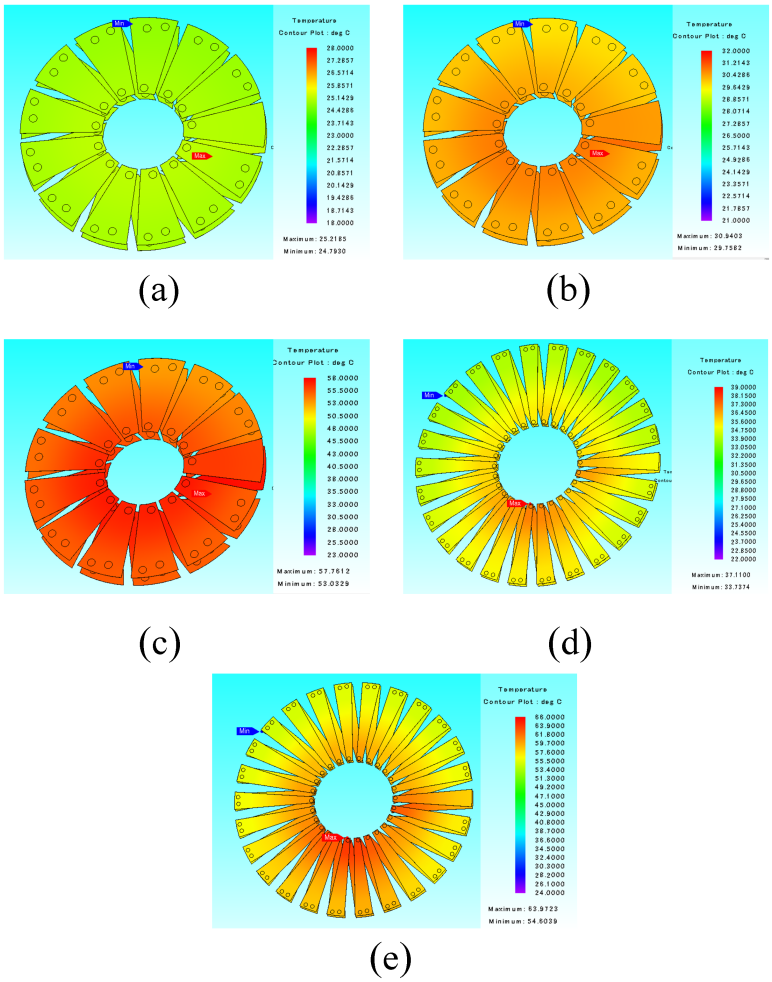

Figure 3.13: Simulation results of temperature rise at different current

These simulations were conducted for 1000 seconds, as it can reach to equilibrium condition. The figure 3.13 (a), (b) and (c) presents 13 turns inductor while applying 3 A, 5 A and 10 A, respectively; and figure 3.13 (d) and (e) presents 26 turns inductor while applying 3 A and 5 A. These are the temperature profiles for all scenarios that has been conducted in this thesis. The temperature rise for 3 A and 5 A current on 13 turns inductor are really low 1$^{\circ}C$ and 5$^{\circ}C$ respectively while in the 26 turns

inductor, for same condition the temperature rise is huge $15°C$ and $41°C$. Since heat transfer is inversely proportional to the thickness of the board, where 13 turns inductor has thickness of $3.5\,mm$, and 26 turns inductor has thickness of $1.5\,mm$. Therefore, temperature rise for 26 turns inductor is much higher than 13 turns inductor. The temperature rise for $10\,A$ current on 13 turns inductor $34°C$ which is as expected to be higher. To prove this analysis, hardware tests were done for the same scenarios which are explained here.

3.7 Experimental Results

Both the designs were analyzed analytically and by simulation, in which they have compatibility in inductance and resistance. After that to prove on hardware, the inductors with 13 turns and 26 turns were designed in PCB design software called Allegro which is shown in figure 3.14 and figure 3.15 respectively. These inductors are tested mainly for thermal analysis and for filtering.

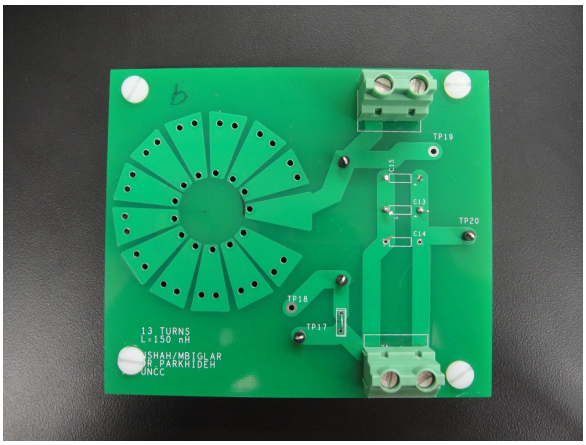

Figure 3.14: 13 turns inductor embedded onto PCB

To measure the value of inductance, Agilent $E4980A$ Precision LCR meter was used which can measure up to $2\,MHz$. For 13 turns inductor, the value of inductance was $132\,nH$ and for 26 turns inductor, the value of inductance was $218\,nH$ which is quite near to simulated values. According the simulations, the value of inductance does not change in high frequency as shown in figure 3.12, these values of inductance

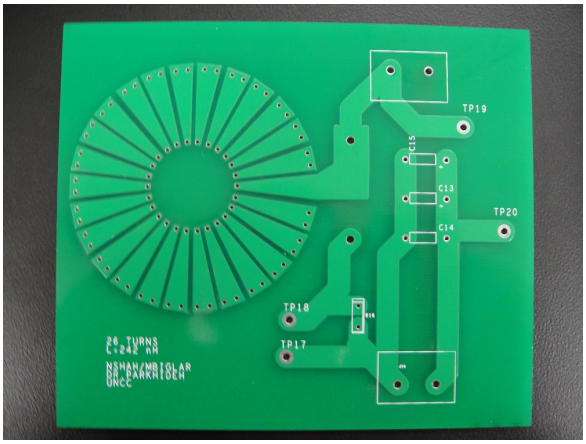

Figure 3.15: 26 turns inductor embedded onto PCB

of 5 MHz can be compared with 2 MHz.

To measure the value of DC resistance, by current source, current was applied to these boards. While applying different currents on the board, stationary multi-meter was used to measure the voltage drop across the inductor. From the basic Ohm's law, resistance can be calculated which is $30 m\Omega$ for 13 turns inductor and $135 m\Omega$ 26 turns inductor and they are near to the simulated results.

3.7.1 Thermal Analysis for Hardware Design

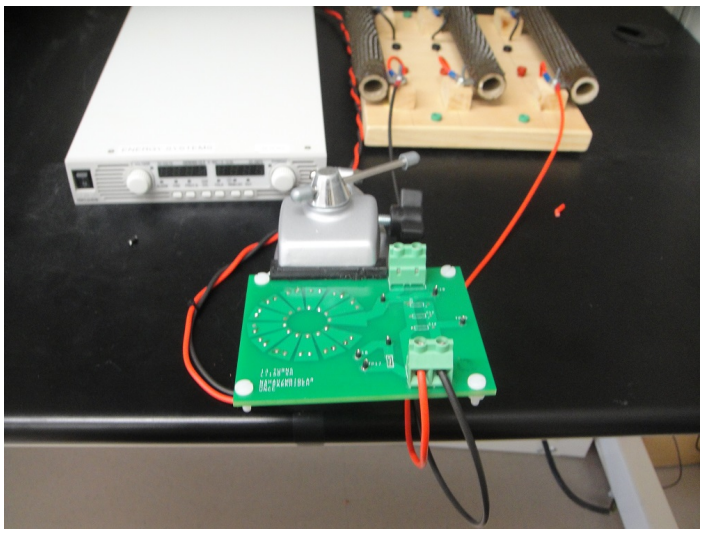

Figure 3.16: Test set up for thermal analysis

In this analysis, both inductor designs were tested for different currents for tem-

perature characteristics and for that, Flir $I60$ thermal camera was used. Here the main advantage of these designs are that heat sink is not required to keep temperature rise in maximum range. As shown in figure 3.16, at the input side of inductor was connected to a current source and output side of inductor was connected to a load that can handle high power. The heat can transfer easily from top and bottom side of inductor board due to holder. 13 turns inductor has been tested for 3 A, 5 A and 10 A, while 26 turns inductor for 3 A and 5 A.

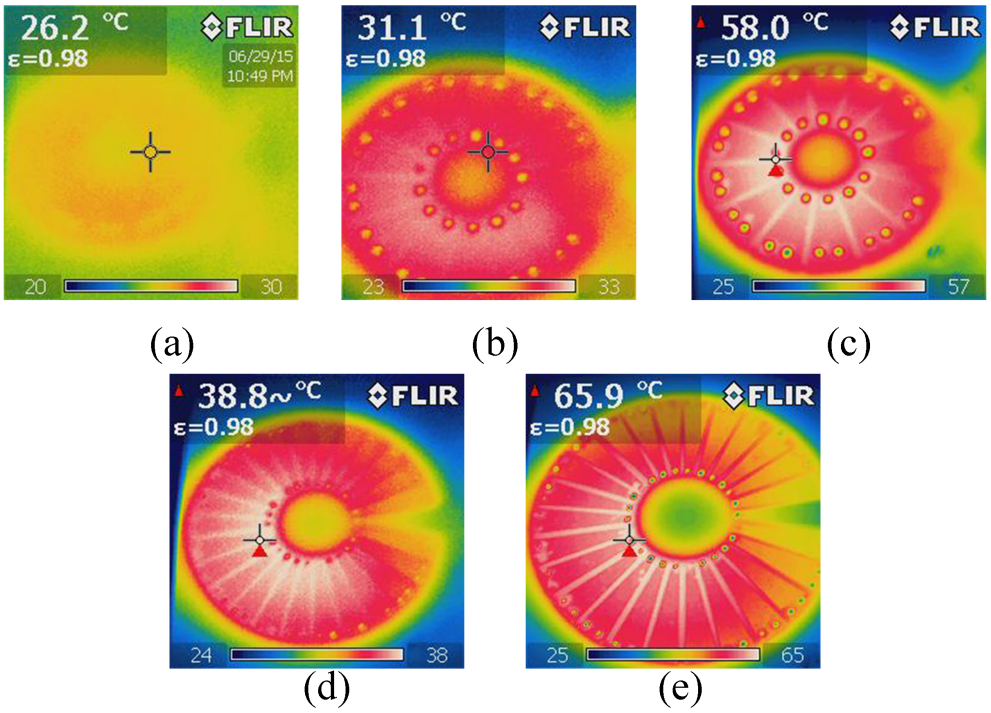

Figure 3.17: (a) 13 *turns* 3 A, (b) 13 *turns* 5 A,(c) 13 *turns* 10 A,(d) 26 *turns* 3 A and (e) 26 *turns* 5 A; Temperature results

The temperature rise results as shown in figure 3.17 are similar to simulated results as shown in figure 3.13. All the scenarios to reach stable equilibrium state ran for at least 15 minutes under constant monitoring of temperature. As expected, the temperature rise in 13 turns and 26 turns at same current 3 A is different, since the inner side length of each petal and diameter of vias are considerably small in 26 turns inductor design. The inner side of petal in every inductor has higher temperature rise

than outer side due ot the length of each side. The same situation happens in the hardware, middle part of inner side inductor gets hotter than other parts of inductor, as near to input and output, heat can be dissipated easily compared to inner side. The temperature rise of vias are $< 40°C$, that means that they are compatible with analytic design. Now, as it can be seen in figure 3.16 and 3.13, the difference of temperature from inner side of top inductor than inner side of bottom inductor is almost $3°C$. The reason behind this asymmetric pattern still needs to be figured out.

3.7.2 Filtering Analysis for Hardware Design

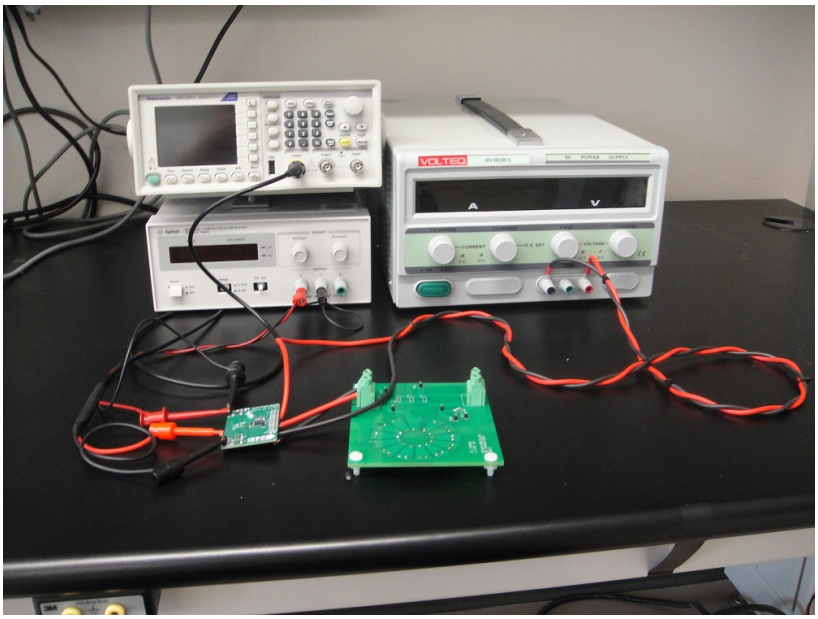

Figure 3.18: Inductor board with converter

These inductor boards have been designed for filtering purpose of high frequency $(5MHz)$ H bridge converter. Efficient Power Conversion (EPC) designs different types of converter for high frequency application with Gallium Nitride (GaN) switches. EPC 9033 eval board was used as a converter throughout this thesis, where EPC 2020 eGaN Field Effect Transistor (FET) used, which has advantages such as lower conduction and switching losses, high power density and low $R_{DS(on)}$ $(2.2m\Omega)$ which means it can operate at high current [22]. The test can be set up as shown in figure 3.18, where

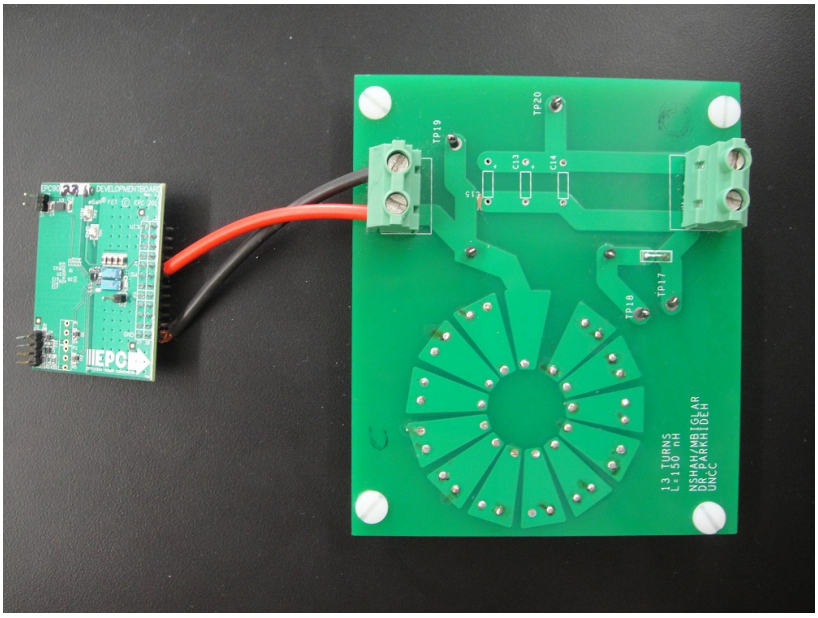

Figure 3.19: Closer view of 13 turns inductor with converter

two different power supplies need to be used, one for gate driver and another for DC bus. The voltage amplitude of function generator should be $3\,V$ to drive the gates. The hardware can be set up as shown in figure 3.18 and 3.19.

Table 3.2: Given parameters to circuit

Parameters	**Value**
Input voltage, Vin	$12\,V$
Duty cycel, d	0.6
Frequency, f	$5\,MHz$
Load, R	$1.5\,\Omega$

As shown in figure 3.18, the output of converter board is connected with inductor board with wire and load is connected to the output of inductor. The applied parameters can be tabulated as shown in table 3.1.

The output voltage for 13 turns and 26 turns inductors are $6.8\,V$ and $6.6\,V$ respectively, as 26 turns inductor have higher resistance. Hence it has higher losses as expected. For 13 turns and 26 turns, according to ripple calculation (3.12), the current ripple should be $3.2\,A$ and $2.4\,A$ respectively. However, due to wiring connection,

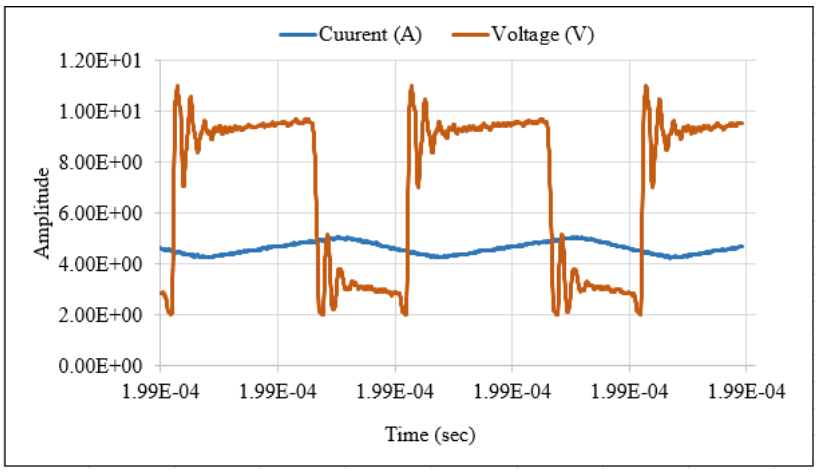

Figure 3.20: Output voltage and current 13 turns inductor board

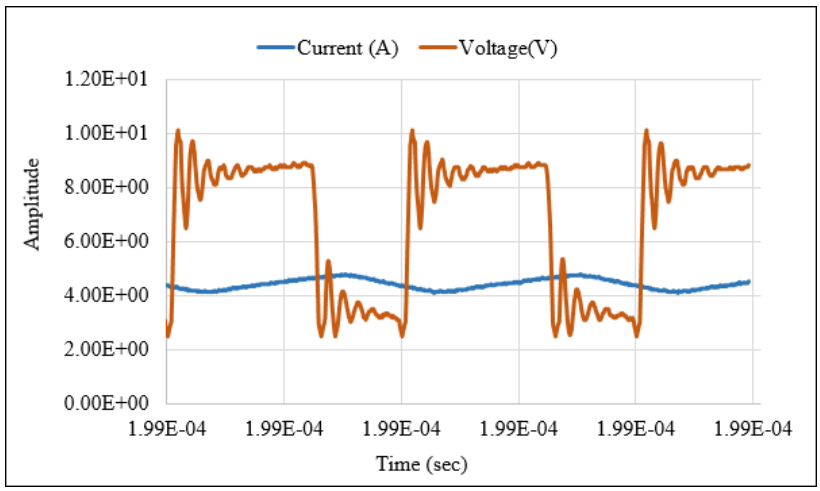

Figure 3.21: Output voltage and current 26 turns inductor

load and traces of the PCB board the inductance increases of the whole circuit. The current ripple decreases as inductance of board increases. The same test has been carried out for different frequencies 1 MHz and 2 MHz. The range of inductance is near to each other. That means inductance value for all operations remain constant for high range of frequency.

$$\Delta I_L = \frac{(V_{in} - Vo) \times D \times T_s}{L} \tag{3.12}$$

where ΔI_L is current ripple, V_o is output voltage and T_S is time which is $1/Frequency$.

According to the equation 3.12, the value of inductance had been calculated, as

Table 3.3: Inductance value according to ripple calculation

Design	**Experimental Results**	**Expected Results**
13 turns	$810\,nH$	$150\,nH$
26 turns	$930\,nH$	$240\,nH$

shown in table 3.3. As it can be seen, the experimental result has much higher inductance than expected results, because of traces of PCB, load and wire which add inductance to the board. For, 13 turns and 26 turns, same connection and loads had been used. Therefore, the difference of inductance value (i.e. external inductance) between expected result and experimental result, for both design is close (approximately $660\,nH$) to each other.

CHAPTER 4: OPTIMIZED DESIGN ANALYSIS

4.1 Introduction

The goal of this optimized design is to pass high current (20 A), miniaturize size and to reach higher efficiency (i.e. losses of inductor should be lower than 1% of total power). To increase efficiency and reduce the size of Switch Mode power Supplies (SMPS), passive components such as inductors and transformers play an important role [4]. To achieve this goal, resistance of inductor needs to be considered as a main factor. The previous chapter (chapter 3) has reported the compatibility of simulation and hardware results for two designs 13 turns inductor and 26 turns inductor, where they have losses around 6 $watts$ at their higher current capacity at 5 MHz switching frequency. This chapter explains the design procedure, merits and challenges of new prototype of inductor.

4.2 Inductor Design

As mentioned in section 4.1, the resistance of inductor is main consideration where basic affecting parameters can be seen from equation 4.1. The resistivity is completely dependent on the material, however the length and area can be chosen according to requirement. In our case, resistance can be reduced by decreasing the length of petal, decreasing the number of turns and increasing the thickness of copper in each layer. However, these parameters affect the inductance value according to equation 3.3. To maintain resonance frequency value according to equation 3.1, the capacitance needs to be adjusted accordingly the inductance value.

$$R = \rho \frac{l}{A} \tag{4.1}$$

where ρ is the resistivity of material, l is length and A is cross section area.

First of all, outer diameter needs to be reduced to miniaturize the size of inductor, to decrease its own resistance and to reduce the size SMPS. To keep the resistance value minimum, the outer diameter and number of turns were assumed initially. After that according to equation 3.2, the diameter of via was calculated which should be capable of passing 20 A current. However, due to the geometry restrictions such as inductance value and inner diameter, the diameter of via needs to be decreased which can handle up to 18 A current. The ratio between inner diameter and outer diameter affects the value of inductance. Due to the restriction of space inner side of the petal, one via can be designed to circulate current at inner side. However, it is possible to consider two vias at outer side of petal, so that they can easily handle the current. The important fact needs to be considered here, the vias near to each other increases stray capacitance. Now, inductor can be designed according to section 3.4. The parameters of optimized design inductor can be tabulated as shown in table 4.1.

Table 4.1: Parameters of optimized inductor

Parameters	**Optimized Design**	**Units**
L	50	nH
N	8	–
d_o	30	mm
d_i	15	mm
R_{DC}	2.75	$m\Omega$
R_{AC}	9.65	$m\Omega$
d_{via}	2.8	mm
h	3.8	mm
ρ	$1.7 \times 10^{-}5$	Ω/mm
T_{trace}	0.144	mm
C_{trace}	1.05	mm
$number\ of\ vias$	22	–

It can be seen from table 4.1, the thickness of copper is increased and length of petal is reduced compared to previous designs (3.1). Here, 4 oz copper was used, that

means thickness of copper is 0.144 mm, which helps to reduce DC resistance and to decrease the temperature rise. Thus, the value of resistance decreased significantly compared to previous two designs. However, inductance value is also lower 42 nH compared to previous designs. The value of capacitance can be increased to 2.2 μF to fulfill the cut-off frequency equation (3.1). Due to the geometry restrictions, the clearance between each petal has to be kept 1.05 mm, which affects the resistance. Higher the clearance, higher the resistance.

4.3 Simulation Analysis and Results

After the successful implementation of previous two design, optimized inductor as shown in figure 4.1 was designed in simulation software to investigate resistance, inductance and temperature rise at different value of current and at different range of frequency.

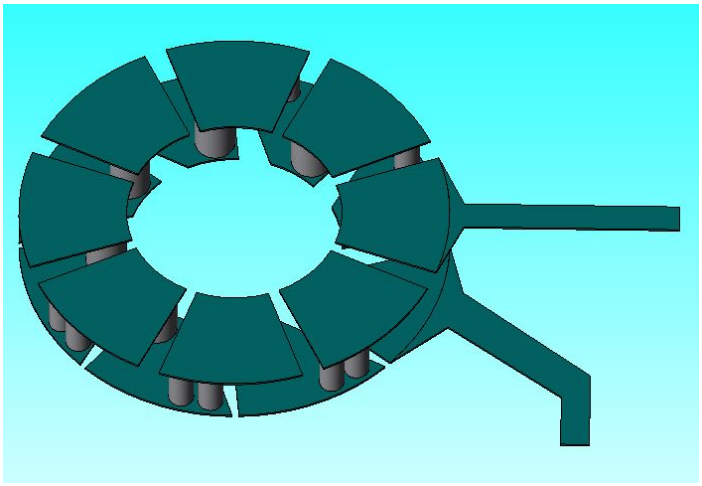

Figure 4.1: $N = 8, L = 50nH$

4.3.1 Calculation of Inductance and Resistance

As described in section 3.6.1, all the necessary settings have been done for this geometry to extract the value of inductance and resistance. The values of resistance and inductance for frequency sweep (1 MHz to 10 MHz) can be shown as figure 4.2 and 4.3.

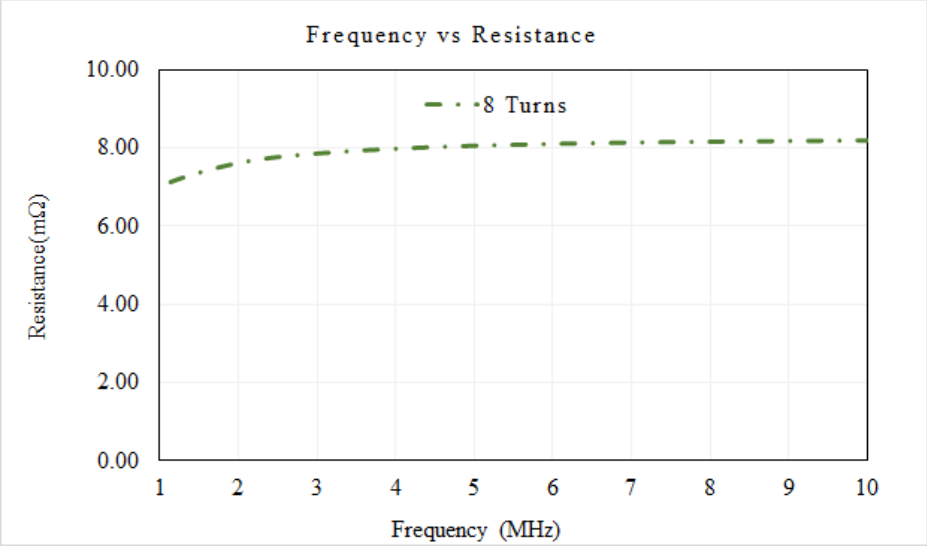

Figure 4.2: Frequency vs Resistance

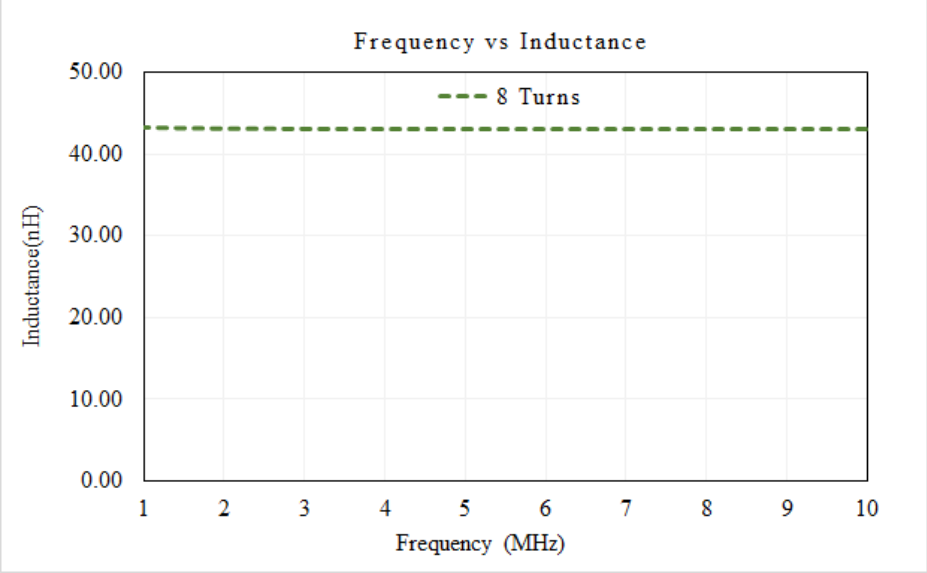

Figure 4.3: Frequency vs Inductance

The simulated value of resistance for low frequency (60 Hz) was 2.96 $m\Omega$, which was predicted, since the calculated value is near to 2.5 $m\Omega$ and 4 oz copper helps to reduce DC resistance. However, at high frequency it increases due to the skin effect and proximity effect. Because of skin effect, the current will flow in skin depth (which can be calculated by equation 2.14) only. That means, current can flow only in the edges of conductor. Hence, AC resistance (can be calculated by equation 3.9)

is around $8\,m\Omega$ at $10\,MHz$ frequency. Due to smaller outer diameter and less number of turns inductance value decrease which is expected. The simulated inductance value is near to calculated value. Therefore, for inductance and resistance, the simulation and calculation are matching. The characteristics of the simulation for this design is as same as previous designs simulation for inductance and resistance 3.12 and 3.11.

4.3.2 Thermal Analysis

All the necessary settings are done according to section 3.6.2. This analysis is conducted for two more scenarios as this inductor is designed for 18 A current.

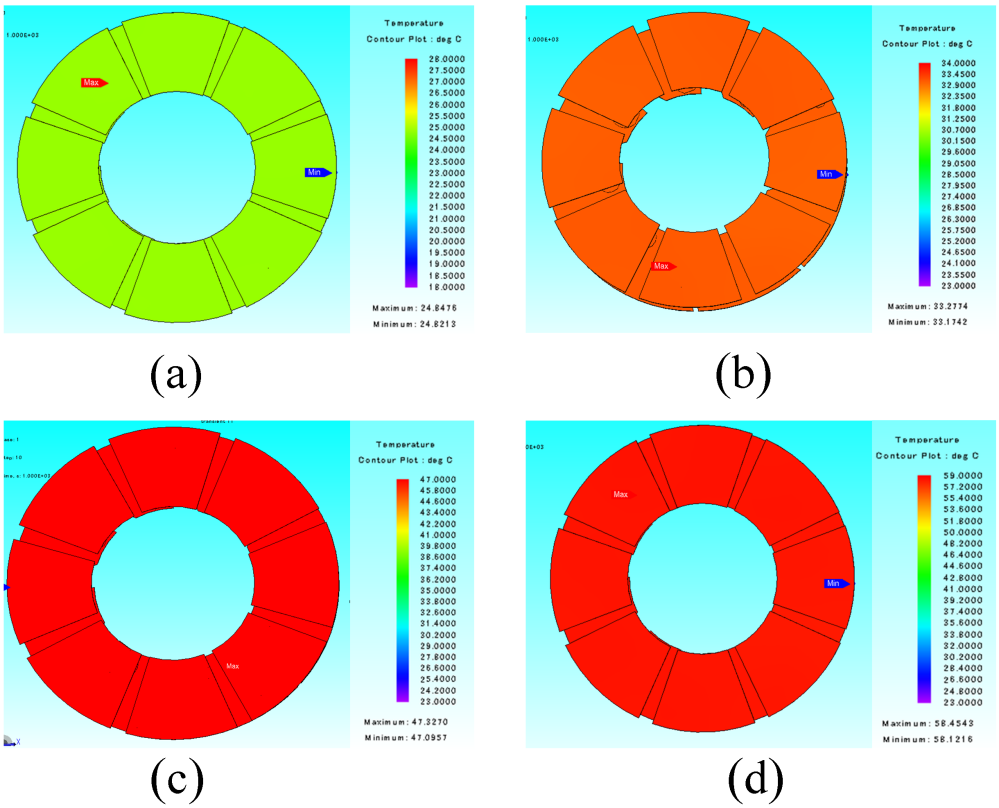

Figure 4.4: Simulation results of temperature rise at different current

The thermal heat transfer coefficient for this design is calculated by equation 3.11, which is 8 $w/m^2\ ^\circ C$. The same as 13 turns inductor, because thickness of board for both design is same. Here, first scenario at $3\,A$ is not shown, since temperature rise at

3 A is less than 0.5 $^{\circ}C$ (which can be negligible). The temperature variations in each case are almost constant. If we consider small temperature difference, then upper left side of inductor gets hotter than other parts.

4.4 Experimental Results

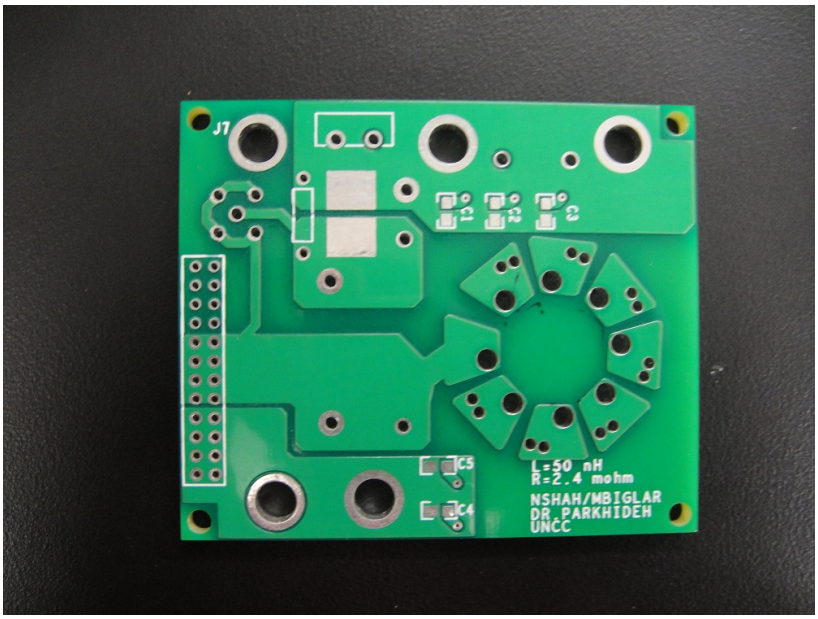

Figure 4.5: 8 turns inductor embedded onto PCB

The same as previous designs, this inductor is designed analytically first and then simulated in JMAG to investigate further. The analytical and simulation results are compatible, therefore, this inductor as shown in figure 4.5 is designed in PCB design software. The bottom side two connectors are used to supply DC voltage to converter and $c4$ and $c5$ is provision for capacitors. The left side 24 pin connectors are used to connect converter directly to inductor board. $c1$, $c2$ and $c3$ are the provision kept for filter capacitance and all the connector in the end are kept for the provision for different size of load. All the vias had been filled so that they can handle more current.

The same as previous measurements, to measure the value of inductance Agilent $E4980A$ Precision LCR meter was used which can measure up to 2 MHz. For 8 turns inductor, the value of inductance was 46 nH, which is quite near to simulated and

calculated values. Since the value of inductance does not change of high frequency as shown in figure 3.12, these values of inductance of 2 MHz can be compared with 5 MHz.

To measure the value of DC resistance, current source was used and current was applied to this board. While applying different currents on the board, stationary multi-meter was used to measure the voltage drop across the inductor. From the basic Ohm's law, resistance can be calculated which is 3.5 $m\Omega$ for 8 turns inductor which is close to simulated and calculated results.

4.4.1 Thermal Analysis for Hardware Design

The same as shown in section 3.7.1, this analysis is done for this design. The test set up is same as shown in figure 3.16. This design is tested for 5 A, 10 A, 15 A and 18 A which is shown in figure 4.6 (a), (b), (c) and (d) respectively. This design is tested for 3 A, but there is no temperature rise for this case.

These results show good agreement with simulation results in temperature rise. The temperature profiles of hardware has some difference than simulated, as in hardware, input and output of inductor has large plane to dissipate heat easily. Hence, input and output side of inductor has a temperature difference of 3°C than other part of inductor. Moreover, 4 oz copper helps to reduce temperature rise. The temperature rise till 18 A stays in the minimum range. For this design, no heat sink is required, so it can be used without any further calculation and investigation.

4.4.2 Filtering Analysis for Hardware Design

For this analysis, the set up is done with converter same as section 3.7.1. There is one main difference from previous design. In the previous design wire is needed to connect inductor board to converter. But, as shown in figure 3.18 and 4.8, new design converter can be directly connected to board. Hence, inductance of that particular wire can be avoided.

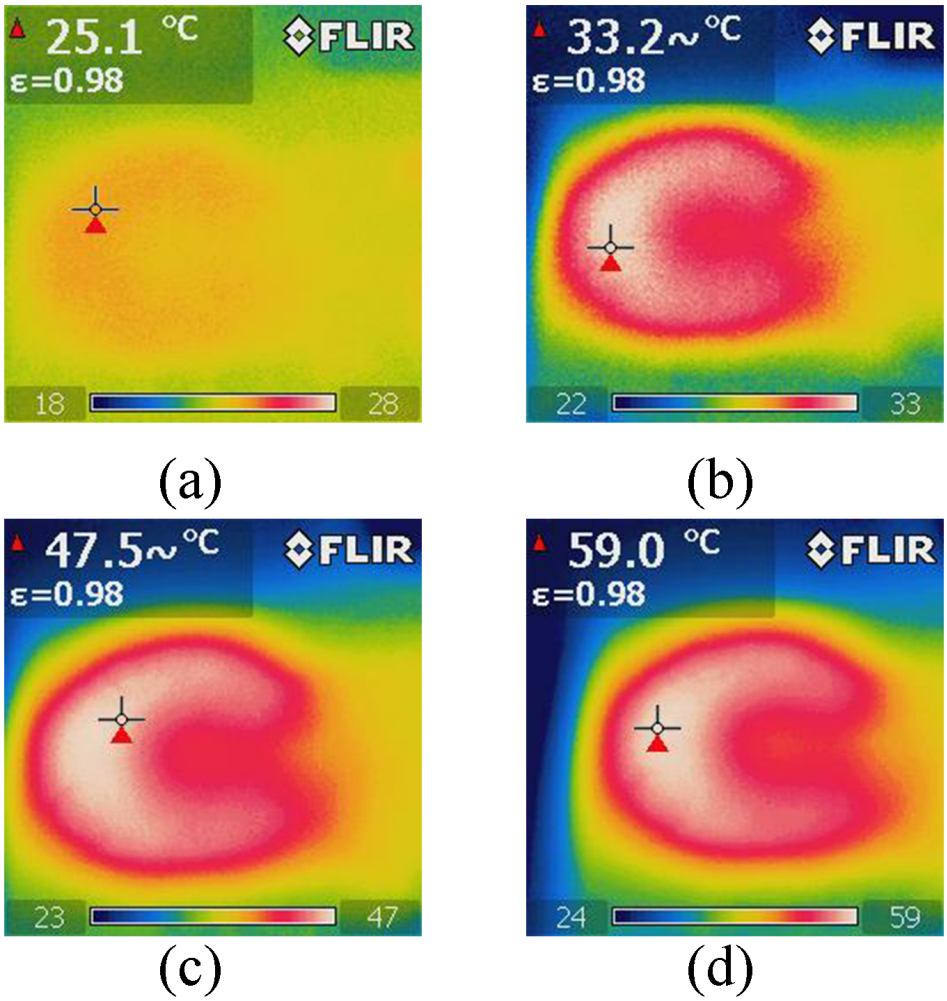

Figure 4.6: (a) 5 A,(b) 10 A,(c) 15 A and (d) 18 A; Temperature results

The given parameter to circuit is same as shown in table 3.1.

The output voltage for 8 turns is $6.8V$. For 8 turns, according to ripple calculation (3.12), the current ripple should be 12 A. However, due to load and traces of the PCB board the inductance increases of the whole circuit. Therefore, the current ripple decreases as inductance of the setup increases. The same test has been done for different frequencies 1 MHz and 2 MHz. The range of inductance is close to each other. That means inductance value for all operations remain constant for high range of frequency. Moreover, compared to previous two designs, voltage reaches to zero value, since in this case converter is operating in Discontinuous Conduction

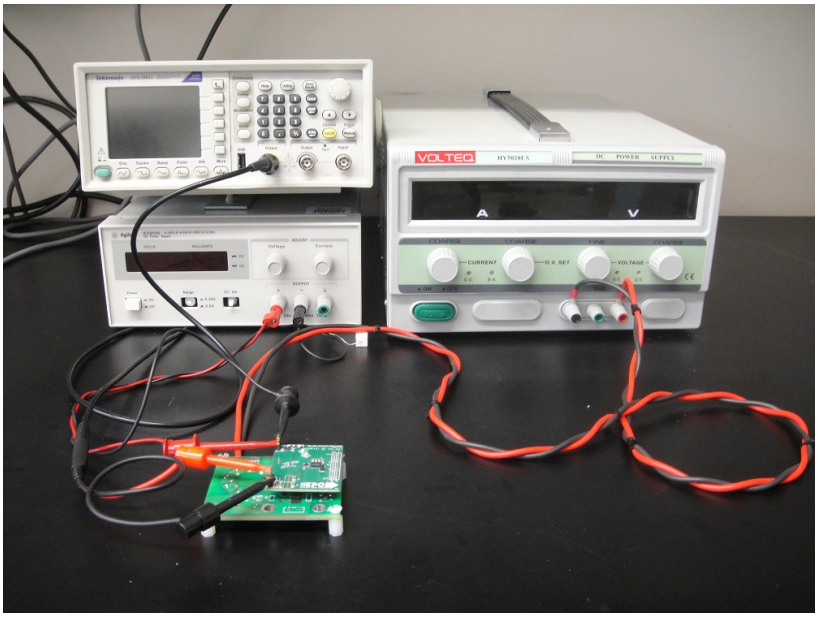

Figure 4.7: The set up of 8 turns inductor board with converter

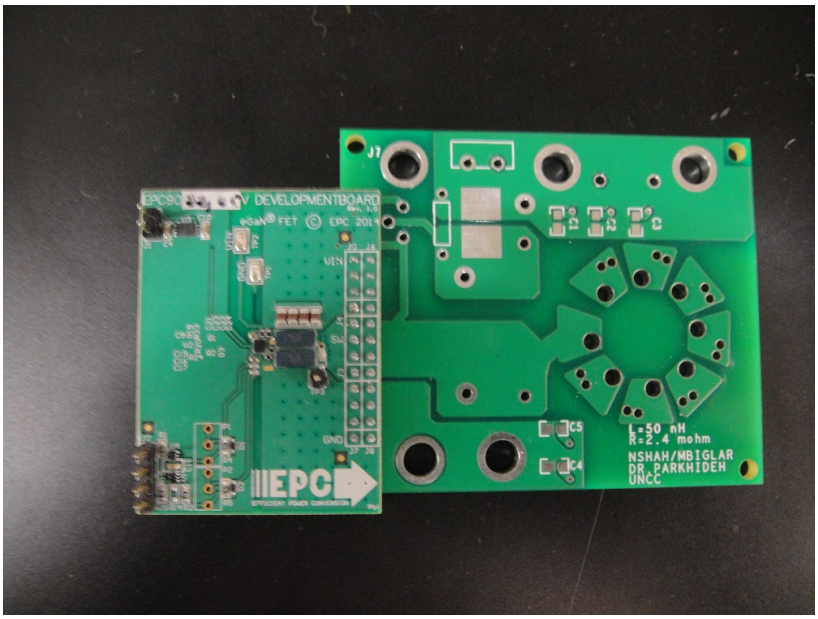

Figure 4.8: Closer view of 8 turns inductor board with converter

Mode (DCM), while in the previous two designs converter operates in Continuous Conduction Mode (CCM). The other condition for DCM is that current ripple should be greater than nominal current, which is applicable for this case.

According to the equation 3.12, the value of inductance had been calculated, as shown in table 4.2. As it can be seen, the experimental result has much higher

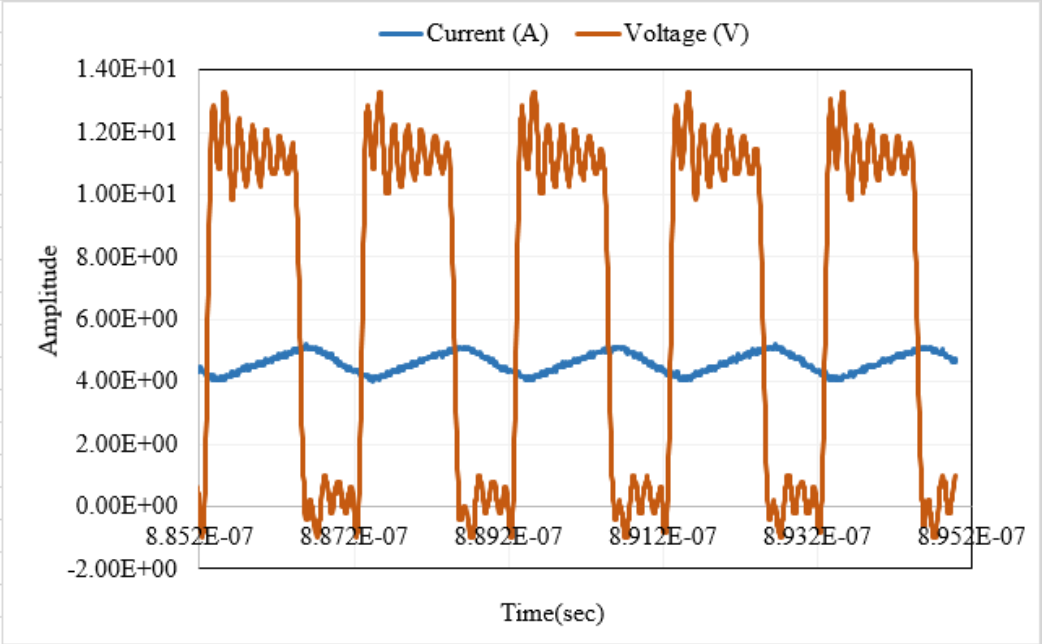

Figure 4.9: Output voltage and current 8 turns inductor

Table 4.2: Inductance value according to ripple calculation

Design	**Hardware Results**	**Expected Results**
8 turns	560 nH	50 nH

inductance than expected results, because of traces of PCB, load and wire which add inductance to the board. However, compared to 13 turns and 26 turns, 8 turns inductor has lower external inductance (510 nH), since converter is directly connected to the inductor board.

CHAPTER 5: CONCLUSION

5.1 Discussion

All three prototypes as shown in figure 5.1 were simulated and tested on hardware for temperature rise, resistance and inductance calculation. For all of them, different analysis have been carried out at different frequency and current.

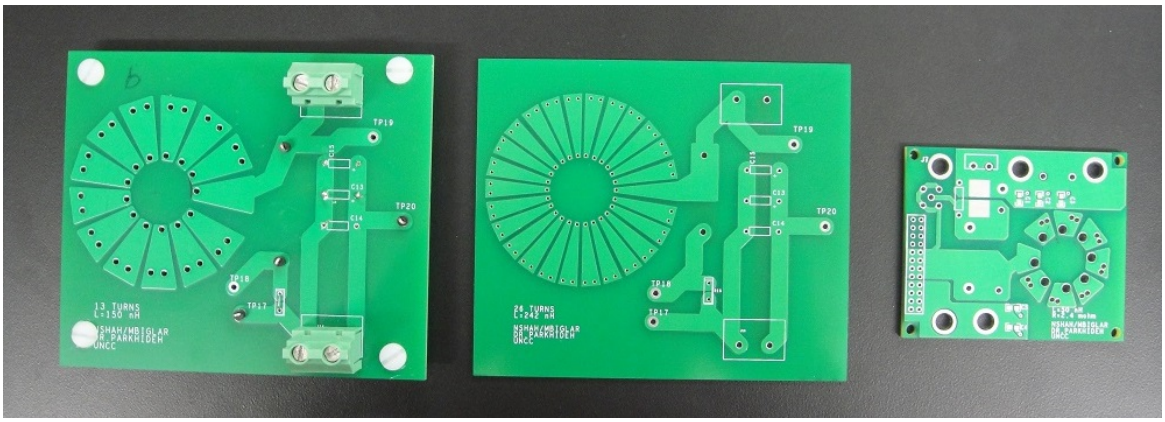

Figure 5.1: All three prototypes of inductor

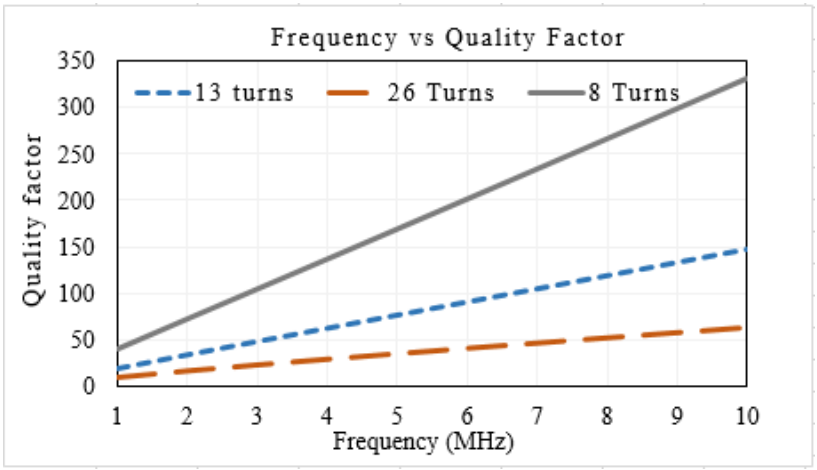

Figure 5.2: Frequency vs quality factor for all three prototypes

The quality factor is a very important parameter which directly implies effective-

ness of an inductor, which can be calculated by equation 2.16. In our case, resistance remains almost constant at frequency sweep of $1\,MHz$ to $10\,MHz$. The quality factor increase with the frequency which can be seen from figure 5.2. Moreover, the resistance of 8 turns inductor is least compared to 13 turns and 26 turns, therefore the quality factor of 8 turns is highest.

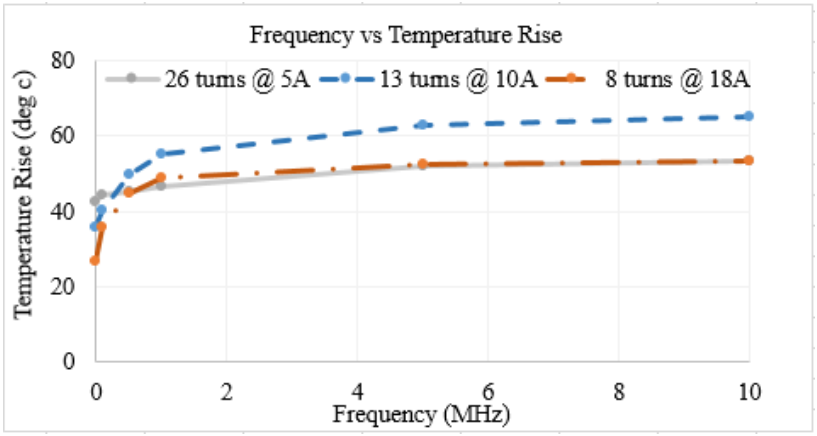

Figure 5.3: Frequency vs temperature rise for all three prototypes

Each prototype is designed for particular current capacity, for instance 26 turns, 13 turns and 8 turns inductors can sustain up to $5\,A$, $10\,A$ and $18\,A$, respectively. These designs were simulated for the highest current which they can handle at different range of frequency from $100\,Hz$ to $5\,MHz$. The maximum temperature rise for each scenario can be shown as figure 5.3. As expected, the temperature rise at higher frequency is higher in every case, since resistance increase with high frequency due to skin effect, which increase temperature rise. It can be seen that, for 13 turns, temperature rise is greater than $40°C$ at $5\,MHz$ frequency. But, for 8 turns and 26 turns, temperature rise remains close to $40°C$ at $5\,MHz$ frequency.

5.2 Summary

This thesis mainly investigated to extract value of inductance and resistance, and analyze of temperature rise for high current (up to $18\,A$) for $5\,MHz$. For that, initially two prototypes (13 turns and 26 turns) were analytically designed for particular in-

ductance and resistance, which are capable of handling $10\,A$ and $5\,A$ respectively, and then simulated in multi-physics software (JMAG) to verify its value. Furthermore, JMAG software has been used for the prediction of temperature rise at different values of current for various frequencies. Then, both prototypes were designed in PCB designer software (Allegro) to verify the calculation at hardware level. All the results are in good agreement with the analytical, simulated and hardware.

The resistance of 13 turns and 26 turns are $55\,m\Omega$ and $205\,m\Omega$ at $5\,MHz$, which have higher losses. Our goal is to design an inductor with losses of $< 1\%$ of total power. Hence, the optimized inductor was designed with 8 turns inductor which can handle up to $18\,A$ current and it's resistance is $8\,m\Omega$ at $5\,MHz$. Therefore, it can satisfy the goal.

The temperature rise of all three prototypes are simulated and tested without using any heat sink. In all of the cases, at their highest current capacity were tested with current source for 15 minutes, so that it can reach to equilibrium steady state. They were simulated for their highest current capacity at frequency sweep of $100\,Hz$ to $1\,MHz$. As expected, for all various scenarios they remain close to $40°C$ temperature rise, except for 13 turns inductor, it goes higher than $40°C$.

5.3 Future Work

This PCB embedded inductor is designed in 2 layers here, it can be designed with 4 layers with the shielding on top and bottom layer to reduce external magnetic field. Furthermore, investigations of EMI can be done in simulation and by experiment.

The temperature rise is predicted without heat sink here, however it can be designed with heat sink to reduce the PCB embedded inductor size.

In this prototype, copper was used as material for inductor, different magnetic materials can be used to shrink the size of inductor. For that purpose, further studies is required to understand the effect of magnetic materials at high frequency.

BIBLIOGRAPHY

[1] Knott, A.; Andersen, T.M.; Kamby, P.; Pedersen, J.A.; Madsen, M.P.; Kovacevic, M.; Andersen, M.A.E., "Evolution of Very High Frequency Power Supplies," Emerging and Selected Topics in Power Electronics, IEEE Journal of , vol.2, no.3, pp.386,394, Sept. 2014

[2] Wenli Zhang; Yipeng Su; Mingkai Mu; Gilham, D.J.; Qiang Li; Lee, F.C., "High-Density Integration of High-Frequency High-Current Point-of-Load (POL) Modules With Planar Inductors," Power Electronics, IEEE Transactions on , vol.30, no.3, pp.1421,1431, March 2015

[3] Orlandi, S.; Allongue, B.; Blanchot, G.; Buso, S.; Faccio, F.; Fuentes, C.; Kayal, M.; Michelis, S.; Spiazzi, G., "Optimization of Shielded PCB Air-Core Toroids for High-Efficiency DCDC Converters," Power Electronics, IEEE Transactions on , vol.26, no.7, pp.1837,1846, July 2011

[4] Madsen, M.; Knott, A.; Andersen, M.A.E.; Mynster, A.P., "Printed circuit board embedded inductors for very high frequency Switch-Mode Power Supplies," ECCE Asia Downunder (ECCE Asia), 2013 IEEE , vol., no., pp.1071,1078, 3-6 June 2013

[5] Sullivan, C.R.; Li, Weidong; Prabhakaran, S.; Shanshan Lu, "Design and Fabrication of Low-Loss Toroidal Air-Core Inductors," Power Electronics Specialists Conference, 2007. PESC 2007. IEEE , vol., no., pp.1754,1759, 17-21 June 2007

[6] Kamby, P.; Knott, A.; Andersen, M.A.E., "Printed circuit board integrated toroidal radio frequency inductors," IECON 2012 - 38th Annual Conference on IEEE Industrial Electronics Society , vol., no., pp.680,684, 25-28 Oct. 2012 doi: 10.1109/IECON.2012.6388746

[7] Erickson, R. W. and Maksimovic, D. (2001), Fundamentals of Power Electronics , Springer .

[8] Ferrite Core Catalog, Magnetics, 2015. Web. (mag-inc.com/design/technical-documents/ferrite-core-documents).

[9] Powder Core Catalog. Magnetics, 2015. Web. (mag-inc.com/design/technical-documents/powder-core-documents).

[10] Wang, Mingliang. Integrated Power Inductors in Silicon for Compact Dc-dc Converters in Portable Electronics. Thesis. University of Florida, 2010.

[11] Hurley, William G., and Werner H. Wolfle (2010), Transformers and Inductors for Power Electronics: Theory, Design and Applications, Wiley.

[12] Swihart, Mark A. "Inductor Cores Material and Shape Choices." Magnetics (mag-inc.com/design/design-guides/inductor-cores-material- And-shape-choices. Magnetics).

[13] JMAG Designer Version 13.1, JSOL corporation (jmag-international.com)

[14] Perreault, D.J.; Jingying Hu; Rivas, J.M.; Yehui Han; Leitermann, O.; Pilawa-Podgurski, R.C.N.; Sagneri, A.; Sullivan, C.R., opportunities and Challenges in Very High Frequency Power Conversion," Applied Power Electronics Conference and Exposition, 2009. APEC 2009. Twenty-Fourth Annual IEEE , vol., no., pp.1,14, 15-19 Feb. 2009 doi: 10.1109/APEC.2009.4802625

[15] Naayagi, R.T.; Forsyth, A.J., "Design of high frequency air-core inductor for DAB converter," Power Electronics, Drives and Energy Systems (PEDES), 2012 IEEE International Conference on , vol., no., pp.1,4, 16-19 Dec. 2012

[16] S. Ramo, J. Whinnery, and T. V. Duzer, Fields and Waves in Communication Electronics 3rd Ed. John Wiley and Sons, INC., 1994.

[17] Zolog, M.; Pitica, D.; Pop, O., "Characterization of Spiral Planar Inductors Built on Printed Circuit Boards," Electronics Technology, 30th International Spring Seminar on , vol., no., pp.308,313, 9-13 May 2007 doi: 10.1109/ISSE.2007.4432869

[18] Small Solar Electric Systems." Department of Energy. N.p., 2013. Web. (energy.gov/energysaver/articles/small-solar-electric-systems)

[19] Bunea, R.; Codreanu, N.-D.; Ionescu, C.; Svasta, P.; Vasile, A., "PCB tracks thermal simulation, analysis and comparison to IPC-2152 for electrical current carrying capacity," Electronic System-Integration Technology Conference (ESTC), 2010 3rd , vol., no., pp.1,4, 13-16 Sept. 2010

[20] JMAG Application Note: Analysis of Impedance-Frequency Characteristics of a Cable (jmag-international.com/catalog/70-cable-impedancefrequencycharacteristics.html)

[21] Charles Mauney, Thermal Considerations for Surface Mount Layouts, Texas Instruments

[22] Lidow, Alex, David Reusch, and Johan Strydom. APPLICATION NOTE: AN017." Fourth Generation EGaN FETs Widen the Performance Gap with the Aging MOSFET (n.d.): n. pag. Web. 2014